Copyright Warning & Restrictions

The copyright law of the United States (Title 17, United States Code) governs the making of photocopies or other reproductions of copyrighted material.

Under certain conditions specified in the law, libraries and archives are authorized to furnish a photocopy or other reproduction. One of these specified conditions is that the photocopy or reproduction is not to be "used for any purpose other than private study, scholarship, or research." If a, user makes a request for, or later uses, a photocopy or reproduction for purposes in excess of "fair use" that user may be liable for copyright infringement,

This institution reserves the right to refuse to accept a copying order if, in its judgment, fulfillment of the order would involve violation of copyright law.

Please Note: The author retains the copyright while the New Jersey Institute of Technology reserves the right to distribute this thesis or dissertation

Printing note: If you do not wish to print this page, then select "Pages from: first page # to: last page #" on the print dialog screen

ABSTRACT

OPTO-MECHANICAL DESIGN OF SYNCHROTRON RADIATION-BASED FAR-INFRARED SPECTROSCOPIC ELLIPSOMETER WITH STRONG MAGNETIC-FIELD

by

Ahmad Abbas Chaudhry

The objective of this dissertation is to present opto-mechanical design of a synchrotron radiation based far-infrared spectroscopic ellipsometer with a strong external magnetic-field capability. Since high magnetic field has enabled major breakthrough in science such instrument will be highly important to the field of condensed matter physics and characterization of advanced electronic materials. This instrument will be installed at the multi-User facility with the most advanced synchrotron light source: Natonal Synchrotron Source (NSLS-II) at Brookhaven National Laboratory (BNL).The proposed here instrument is capable to measure full Mueller matrix spectroscopic ellipsometry spectra in high magnetic fields of up to 9 Tesla. The designed instrument consists of Polarization State Generator (PSG) chamber, Spectromag optical solenoid (high magnetic field up to 9 T), cryogenic sample stage, Polarization State Analyzer (PSA) chamber, and a bolometer. The PSG and PSA vacuum chambers are separated from the magnet volume with two pairs of gate valves equipped with optical windows. This instrument is capable of using synchrotron radiation in the spectral range of 20 cm-1 and 4000 cm-1. The sample stage could operate in the low temperature range down to 4 K with an option to cool sample down to 1.6 K. This instrument allows User to switch between Faraday and Voigt configurations for external magnetic field. This ellipsometer will be able to measure the full-Mueller matrix spectra using rotating retarders and rotating polarizers.

OPTO-MECHANICAL DESIGN OF SYNCHROTRON RADIATION-BASED FAR-INFRARED SPECTROSCOPIC ELLIPSOMETER WITH STRONG MAGNETIC-FIELD

by
Ahmad Abbas Chaudhry

A Thesis
Submitted to the Faculty of
New Jersey Institute of Technology
in Partial Fulfillment of the Requirements for the Degree of
Masters in Physics

Department of Applied Physics

January 2016

APPROVAL PAGE

OPTO-MECHANICAL DESIGN OF SYNCHROTRON RADIATION-BASED FAR-INFRARED SPECTROSCOPIC ELLIPSOMETER WITH STRONG MAGNETIC-FIELD

Ahmad Abbas Chaudhry

Dr. Andrei Sirenko, Thesis Advisor Department Chair and Professor of Physics, NJIT	Date
Dr. Tao Zhou, Committee Member Associate Professor of Physics, NJIT	Date
Dr. Leonid Tsybeskov, Committee Member Department Chair and Professor of Electrical and Computer Engineering, NJIT	Date
Dr. Trevor A. Tyson, Committee Member Distinguished Professor of Physics, NJIT	Date

BIOGRAPHICAL SKETCH

Author: Ahmad Abbas Chaudhry

Degree: Master of Physics

Date: January 2016

Undergraduate and Graduate Education:

- Master of Science in Physics,
  New Jersey Institute of Technology, Newark, NJ, 2016

- Bachelor of Science in Mechanical Engineering,
  New Jersey Institute of Technology, Newark, NJ, 1999

Major: Applied Physics

Presentations and Publications:

Ahmad Abbas Chaudhry and Paul F. Freisinger, "Method and Apparatus for Manually Opening a valve with a Tolerance Compensating Stem," United States Patent And Trademark office Reference No. 0021984-034US, Filed December 30 2009.

بسم الله الرحمن الرحيم

لا إله إلا الله محمد رسول الله

"In the name of Allah the most Merciful the Compassionate, there is no God but the One, no partner has He, Muhammad is the Messenger of Allah." (Quran)

I am first and far most thank full to Allah (God almighty) for allowing me to understand his creations and benefit from it. I am greatly thank full to my family, my beloved wife Aasyia for her help and patience during my masters study. I am thank full for my loving kids Arwa, Musa, Zainab, and Musa. I am thank full for my parents, there love and guidance throughout my life.

To my loving Family and Friends

ACKNOWLEDGMENT

I would like thank my advisor, Dr. Andrei Sirenko for his great help and guidance during my studies and in the completion of this thesis. I greatly appreciate how patiently and kindly he has worked with me. I have in particular liked the ways he has taught me, by asking simple questions that made me think. I have learned so much.

I would like to thank committee members, Dr. Andrei Sirenko, Dr. Tao Zhou, and Leonid Tsybeskov, for their participation and feedback. It is only their guidance that has allowed me to learn so much and succeed in the completion of the thesis. Dr. Tao Zhou, I was very happy to have all the physics classes him. He was a great teacher and I enjoyed each and every lecture in his classes.

I would also take this opportunity to thank my employer ASCO Numatics (Emerson Industrial Automation) for its financial support. I appreciate my managers allowing me a flexible schedule during my studies.

TABLE OF CONTENTS

Chapter	Page
1 INTRODUCTION……..…….	1
1.1 Objective …….....……..……...	1
1.2 Background Information …….…….…...	2
1.3 Importance of the Synchrotron Radiation for Far-IR Ellipsometry ……	5
2 CURRENT STATE of the ART in SYNCHROTRON RADIATION BASED ELLIPSOMETRY and POLARIMETRY……..……	8
2.1 Introduction ……..……	8
2.2 Review of Existing Ellipsometers at the Synchrotrons……	11
2.3 Proposed Magneto-MM-SE at MET NSLS-II *vs*. the Previous One at U4IR-NSLS….	12
2.4 Existing Magneto-Ellipsometers with Laboratory Light Sources ……..	13
2.5 Review of the Existing Far-IR Magneto-Optical Transmission-Reflection Setups in US and Europe ……..…….....	14
3 FUNDAMENTALS of MM ELLIPSOMETRY and its APPLICATION to MULTIFERROICS……	17
3.1 Basics of Bi-anisotropic Materials and Light Propagation in Bi-anisotropic Medium ……..…….....	17
3.2 METHOD: Combination of MM-SE and 4×4 Berreman's Simulation Approach …….……...…	22
3.3 Basics of the Muller Matrix Spectroscopic Ellipsometry (MM-SE) ……..	13
3.4 Berreman's 4x4 Matrix Propagation Technique for Optical Spectra Analysis …	23
3.5 Importance of using both Faraday and Voigt Field Configurations in the Same Experimental Setup …….…...	27
3.6 Recent Accomplishments in MM-SE using Far-IR Synchrotron Radiation ……	30

4 DESIGN of OPTO-MECHANICAL DESIGN of SYNCHROTRON RADIATION-BASED FAR-INFRARED SPECTROSCOPIC ELLIPSOMETER WITH STRONG MAGNETIC-FIELD…….. 32

4.1 Components and Technical Details for SR-MM-SE ……...……. 32

4.2 Mechanical Solutions …….….. 34

4.3 Magnetic Field Solution ……... 46

4.4 Vacuum Solution …….……. 49

4.5 Solutions for the Sample Cooling to Low Temperatures ……. 53

4.6 Optical Solution/ Light Propagation …… 54

4.7 Ellipsometry Solution …….. 56

5 CONCLUSION ……..……... 57

APPENDIX WITH DRAWINGS ……. 59

REFERENCES 70

CHAPTER 1

INTRODUCTION

1.1 Objective

The objective of this dissertation is to present opto-mechanical design of a synchrotron radiation based far-infrared spectroscopic ellipsometer with a strong external magnetic-field capability. The proposed here design is unique in terms of a wide verity of experimental capabilities to conduct accurate experiments with magnetic materials. This instrument will be installed at the multi-User facility with the most advanced synchrotron light source: Natonal Synchrotron Source (NSLS-II) at Brookhaven National Laboratory (BNL). This high-brightness light source is chosen to resolve the optics throughput limitations of the ellipsometry technique that uses glancing angle light incidence at the sample surface. The proposed here instrument is capable to measure full Mueller matrix spectroscopic ellipsometry spectra in high magnetic fields of up to 9 Tesla.

The optics components are selected to perform optimally from far- IR to near-IR spectral range: between 20 cm^{-1} to 4000 cm^{-1}. This instrument allows the user to switch between Faraday and Voigt configurations at very low temperature of 4.2 K with an additional option of cooling the samples as low as 1.6 K. Future Users will be able to configure optics for the Polarization State Generation (PSG) and Polarization State Analyzer (PSA) sections using removable optical trays. The PSG and PSA vacuum chambers are separated from the magnet volume with two pairs of gate valves. One gate valve in the pair is equipped with an ultrathin mylar window for measurements and another gave valve is equipped with a thick quartz window for convenient optical

alignment. Our unique opto-mechanical approach to use windows mounted on the gate valves and the side-load of the samples through the window port of the magnet will enable ellipsometry measurements without detrimental depolarization effects from the cold cryostat windows.

1.2 Background Information

The recently written report by the National Research Council on "High Magnetic Field Science and Its Application in the United States: Current Status and Future Directions", states that high magnetic fields have enabled major breakthroughs in science [1]. In condensed matter physics, high magnetic fields, in competition with internal magnetic forces, can create exotic magnetic states in advanced electronic materials, especially if experiments are conducted at low temperatures. The nature of these exotic electronic states challenges our basic understanding of matter. For example, the field can create a "spin-ice" phase that exists only in magnetic matter. These exotic magnetic states also provide insight for future materials applications. Among these states are phases with spin-charge interactions needed in next-generation electronics and spintronics. The availability of the high magnetic fields complements the development of novel materials. In the next 10 years, new materials possessing topological phases and useful functionalities will be advanced by their study in high fields. The aforementioned report of the National Research Council contains strong recommendations for the further development of all-superconducting, hybrid, and higher field pulsed magnets and their implementation at the advanced photon and neutron sources, such as for example, NSLS-II at BNL.

Photons are one of the most important probes of high-field phenomena, ranging from magnetic resonance, which is of importance to all disciplines including biology, chemistry and physics, to excitation spectra in quantum solids, a central theme of modern condensed matter physics. Over the last decade, the use of photons for control as well as diagnostics of matter has become a major theme for condensed matter physics. Photon sources in the frequency range 0.5 to 25 THz (15 – 700 cm^{-1}) are of special importance for high-field experiments, as typical frequencies of electron spin resonances, cyclotron resonances and phonon features fall in this range. Spectroscopic Polarimetry and Mueller matrix spectroscopic ellipsometry (MM-SE) in particular is the most advanced realization of the IR optical methods applied to Condensed Matter Physics. This approach is significantly more sensitive to materials properties in comparison with conventional transmission-reflection spectroscopy. While the latter measures the energy of elementary excitations that are affected by the magnetic field in the second order perturbation theory, polarimetry measures not only the energy but also the phase changes associated with the selection rules for IR excitations. The phase changes are affected by the magnetic field in the first order of the perturbation and thus are more sensitive to weak magnetic effects.

The new magneto-ellipsometer will be used primarily for magnetic samples, where Users of the instrument expect to observe spin orientation transitions and magneto-electric effects. The future Users of the proposed magneto-ellipsometer will be attracted to this new beamline facility at the National Synchrotron Light Source (NSLS-II) at Brookhaven National Laboratory (BNL) by the unique combination of projected experimental capabilities, such as strong magnetic fields *H*, cryogenic sample

temperatures *T*, and versatile geometries of the measurements including variable angles of incidence (AOI) between the sample surface and the light propagation direction. Thus, the combination of these parameters {*H*, *T*, AOI} with the spectral capabilities of the light source at the MET beamline at NSLS-II determines the merit of the proposed development. The proposed setup will also allow the measurements on the magnetooptical effects on materials with strong spin-orbit coupling, which are the subject of a flurry of research activities, as they host novel states, such as J=1/2 Mott insulators Sr_2MnO_4, topological insulating states, Chern metals, *etc*, where the magnitude of linear bi-anisotropic optical effects (without dissipation they are just the well-known Faraday or Voigt effects) is determined by the spin-orbit coupling.

In this theses we will describe a new design for a multi-User facility for magneto-MM-SE with the following performance features:

- Multi-User Facility at
- The most advanced synchrotron source, such as NSLS-II, BNL for
- Mueller matrix spectroscopic ellipsometry in
- High magnetic field (up to 9 T) and capable to
- Switch between Faraday and Voigt configurations at
- Sample temperatures as low as 4.2 K with an option to cool down to 1.6 K.

1.3 Importance of the Synchrotron Radiation for far-IR Ellipsometry

The exceptional brightness of the synchrotron light source exceeds that for a conventional thermal source (T=1200 K) by a factor of 1000 for wavelengths longer than 10 microns where the source has diffraction-limited dimensions [2]. This is crucial for throughput-limited optical techniques such as microscopy and ellipsometry. Ellipsometry requires a well-defined AOI on the sample such that the numerical aperture (NA) is limited to small values of about 0.05, or f#20. Thus, the diffraction-limited spot on the sample at a far-infrared frequency of 50 cm^{-1} (0.2 mm wavelength) is 0.2 mm/0.025 = 8 mm. In other words, a sample with dimension of ~10 mm would result in a diffraction-limited throughput condition in the far-IR spectral range. The situation becomes even more challenging when a large AOI of about 75 deg is needed for good ellipsometric sensitivity to, for example, a strong metallic response in high-temperature superconductors. Preparing large, high quality samples of correlated magnetic oxide materials can be challenging, so effectively all far-IR ellipsometry measurements have very low throughput. As demonstrated first by Kircher *et al*. in 1997, high brightness synchrotron radiation overcomes this throughput limit and allows for relatively quick ellipsometric measurements of the samples with a modest cross section area of a few mm^2. Synchrotron radiation spectroscopy becomes increasingly important for researching complex oxides where competing orders drive new physical phenomena (*e.g.*, superconductivity, colossal magneto-resistance, multiferroicity). Understanding these materials can require probing the multi-dimensional parameter space of temperature, external magnetic field, pressure and orientation (*e.g*. for anisotropic

crystals); a potentially impractical measurement task without access to the rapid data collection rates at the synchrotron radiation facilities. Synchrotron radiation allows a dramatic decrease of the measurement time that is usually limited not by the signal-to-noise ratio but just by the speed of the equipment motors. For example, recently it has been demonstrated by T. Stanislavchuk *et al*. in 2013 using an ellipsometer at U4IR that a complete measurement of the temperature dependent pseudo dielectric function for one sample orientation can be accomplished in less than one day. This measurement speed is acceptable for most of the modern condensed matter experiments.

To overcome the optics throughput limitation, a high-brightness source, such as MET at NSLS-II, is required for our Project. Our new ellipsometer will be installed at the MET beamline, which is under construction at NSLS-II now. This beamline is expected to become available for Users in 2017. The MET beamline is dedicated primarily to Magneto optics (M), including both, ellipsometry (E), and Time-resolved (T) pump-probe spectroscopy, where (M+E+T) = MET. The characteristics of the light at the MET beam line will define many of the ellipsometer's spectroscopic capabilities. The infrared light, produced as dipole bending magnet radiation, is extracted from the storage ring. The collected beam is transported by an optical system based on a pair of matched ellipsoidal mirrors that produce a 1:1 image of the source at a wedged diamond window. This window isolates the UHV synchrotron environment from the rough vacuum of the beam line spectrometer and other instruments. The beam extraction optics is designed to perform optimally from far-IR to near-IR spectral range, *i.e*., between ~20 cm^{-1} and 4000 cm^{-1}. The low-frequency cut off will be determined by several factors, such as the NA of

the diamond window between the storage ring and the beam line, NA of the magnet, and by the typical size of the samples. The high-frequency cutoff is determined by the available optical detectors, beam splitters of the spectrometer, and ellipsometer polarizers.

CHAPTER 2

CURRENT STATE of the ART in SYNCHROTRON RADIATION BASED ELLIPSOMETRY and POLARIMETRY

2.1 Introduction

This chapter describes several ellipsometry facilities and compares our proposed design to the state of the art in experimental ellipsometry and polarimetry available today. The main benchmark for our design is the previous spectroscopic ellipsometer that has been installed at NSLS-BNL in 2010. In early 2011, that instrument has been open for general user access. It was already able to measure a full-Mueller matrix $\widehat{M}_{ij}$ of anisotropic samples by combining spectral measurements at different orientations of the wire-grid polarizers and rotating compensators, as described by Hauge [3]. Fourier-transform infrared (FT-IR) spectrometer is used for a simultaneous multi-wavelength data acquisition. The theory of the data analysis and spectra simulations has been is described in Reference [4]. The principles of the rotatable broad-band retarders are published in References [5,6]. Recent experimental results for ellipsometry of a broad class of anisotropic and correlated materials have been published in References [7,8,9,10,11,12,13,14,15]. Figures 2.1and 2.2 show the general view and the schematics of the previous generation of the Ellipsometer at U4-IR, NSLS-BNL.

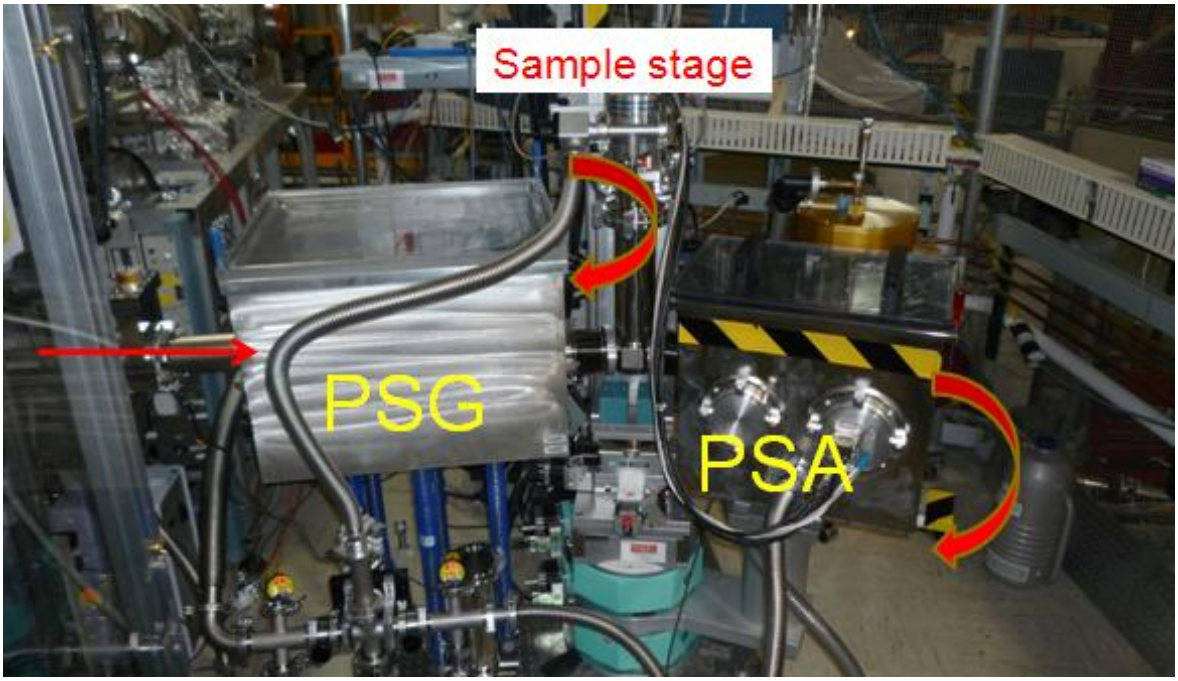

Figure 2.1 Ellipsometer at U4IR beamline consists of three major components: Polarization State Generation (PSG) section, Sample stage with an optical cryostat, and Polarization State Analyzer (PSA) section. Straight red arrow shows light propagation direction from a Bruker spectrometer towards Ellipsometer. Sample Stage and PSA section can accommodate the variable AOI measurements.

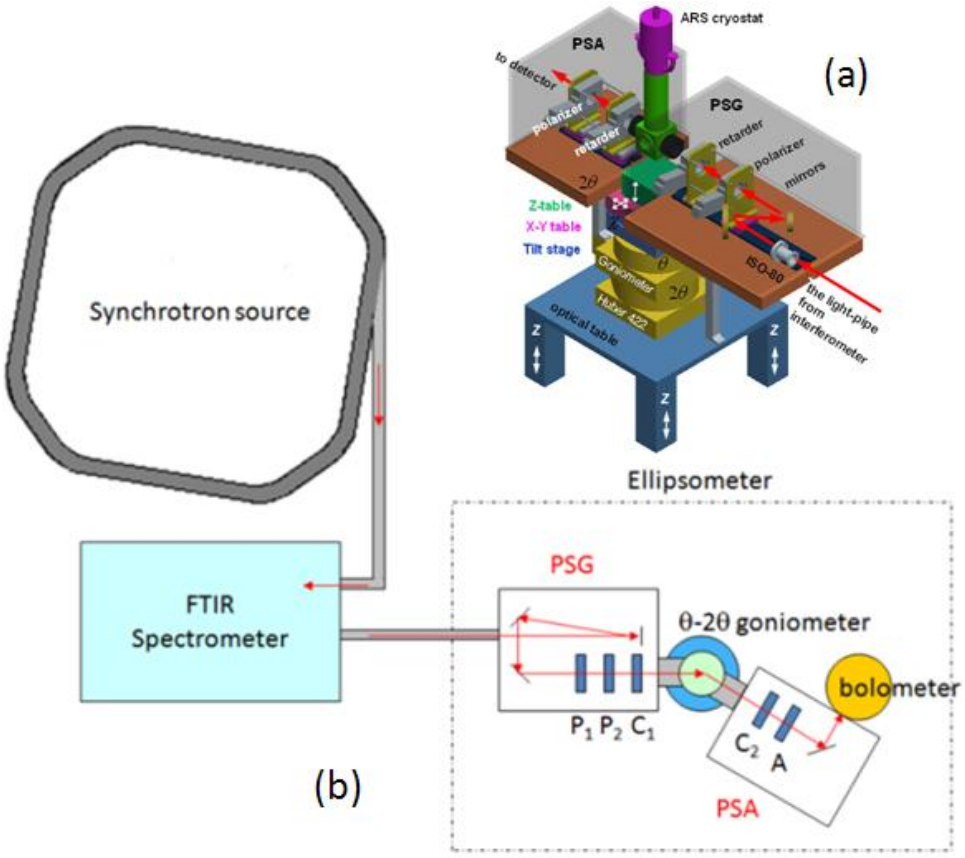

Figure 2.2 (a) a 3D CAD schematics of the far-IR Ellipsometer at U4-IR beamline, NSLS-BNL in the standard configuration, which consists of PSG and PSA sections, sample stage (ARS or OXFORD optical cryostat and HUBER positioning system) The optical cryostat is mounted on the θ- table of the goniometer. The PSA section and bolometer are mounted on the 2θ-arm of the goniometer. The PSG optical section of the Ellipsometer shares the raw vacuum with the interferometer.

(b) Schematics of the light propagation between the synchrotron source, Spectrometer, PSG, and PSA sections of the Ellipsometer. PSG section consists of a retarder C_1, two linear polarizer, P_1 and P_2, and three mirrors: an off-axis parabola with effective focus length of 1 m and two flat ones. PSA section consists of a compensator C_2, linear polarizer (analyzer) A, and a parabolic mirror for light focusing on a bolometer or a CuGe detector [8].

2.2 Review of Existing Ellipsometers at the Synchrotrons

Synchrotron radiation (SR) based far-IR spectroscopic ellipsometry is a versatile technique for materials studies, which has been developed at several SR facilities. The first ellipsometry experiments at NSLS-BNL, which began in the mid 90's, had been initiated in early 90's at the Prof. Cardona's Department of the Max-Planck-Institute für Festkörperforschung (MPI-FKF). The design of the first generation of the far-IR ellipsometer for SR measurements was described by J. Kircher [16] and R. Henn [17]. The first instrument was designed and assembled at MPI-FKF and then installed at NSLS-BNL. The MPI-FKF ellipsometers was equipped with a rotating analyzer and a stationary retarder. The spectroscopic ellipsometry activity at NSLS-BNL reached its peak between 1997-2002, as reflected in a number of publications by the group of C. Bernhard *et al*. [18,19,20,21] After 2003, the ellipsometry activity in the field of strongly correlated systems and high-temperature superconductivity was transferred from NSLS to ANKA, Forschungszentrum, Karlsruhe, Germany [22,23,24,25,26,27,28,29,30]. The design of the far-IR ellipsometers at ANKA, which is similar to that of MPI-FKF, is described in Ref. [31]. The research group of M. Schubert initiated another interesting SE program at BESSY II, Berlin, Germany. The first ellipsometer setup capable of doing measurements in the external magnetic field using SR was described by T. Hofmann et al. [32]. This ellipsometer employed both rotating analyzer ellipsometry (RAE) and truncated measurements of the 3×3 upper left block of normalized MM in the spectral region from 30 to 650 cm^{-1}. Another approach to THz ellipsometry at the synchrotron source was described by A. Röseler *et al*., in Ref. [33]. That ellipsometer was based on a Martin-Puplett (MP) interferometer. All Stokes parameters of the polarized light can be

determined without the need of a retarder as a phase shifting device. This setup has been tested in the spectral range below 1.5 THz employing synchrotron radiation at BESSY from a bending magnet as a dipole radiation source. Finally, in 2010 a new full Mueller Matrix spectroscopic ellipsometer has been commissioned at U4IR beamline of NSLS-BNL by the group of Prof. Sirenko, NJIT [8].

2.3 Proposed Magneto-MM-SE at MET NSLS-II *vs*. the Previous one at U4IR-NSLS

The main qualitative difference between the new design and the old version of the ellipsometer at U4IR beamline of NSLS-BNL is the magnetic field capability. The old ellipsometer was installed at the U4IR beamline, which had a possibility to utilize an old LHe-cooled 10 T optical magnet. That magnet could, in principle, be used for magneto-ellipsometry. However, it turns out that utilization of the existing old 10 T magnet would require a completely new set of the sample loading, vacuum, optical, and mechanical components. More than that, the team of users quickly realized that the cost of continuous operation of the LHe-cooled magnet becomes prohibitively expensive: ~$200/day just to keep the magnet cold. Thus, a new LHe-free setup with the magnet as a central piece for the MET beamline is designed and proposed here. The new Ellipsometer will have an option to switch between Faraday and Voigt configurations that require ~ 4 days due to warm up /cool down maintenance cycle.

2.4 Existing Magneto-Ellipsometers with Laboratory Light Sources

It should be mentioned that utilization of strong magnet for IR spectroscopy has been already implemented in several Reseach Labs using conventional light sources, such as globars, back-travelling wave lamps, and Hg lamps. Two of the most interesting MM ellipsometers with magnetic field capability are the systems recently developed by Shubert, Woollam, Hofmann, Darakcheeva *et al*. and installed at University of Nebraska-Lincoln and Linkoeping University [34,35,36]. Using magnetic field of up to 8 T and a set of the Lab light sources these instrument covers the spectral range from 3 to 7000 cm^{-1} and up to UV range and measure truncated 3×3 blocks of the MM components. Among recently measured materials are relatively large samples, such as epitaxial graphene grown on 6*H*-SiC, Te doped bulk GaAs, and an AlGaN/GaN high electron mobility transistor structures. Note, however, that both of these setups are using cold windows in a 90-deg reflection configuration with AOI=45 deg, which is far from the optimal value of AOI usually chosen to be close to typical sample's Brewster angle of about 70 deg. Some of the experimental spectra from these aforementioned ellipsometry setups have been presented in a form of the *relative* MM components, *i.g.*, $m_{ij}(H)/m_{ij}(H=0)$. One can assume that the cold internal windows of the VTIs introduce significant experimental errors for the measurement of un-normalized $m_{ij}(H)$ spectra that are the most valuable for precise theoretical modeling of ME effects. In addition, we should mention here that the magnetic field is obviously applied there at an angle of 45 deg with respect to the sample surface, which is neither Faraday not Voigt configuration thus introducing an

additional complication for the future studies of ME effects in *e.g*, orthorhombic and hexagonal multiferroics.

2.5 Review of the Existing Far-IR Magneto-Optical Transmission-Reflection Setups in US and Europe

The Quantum Materials Group from University of Geneva, Switzerland lead by Profs. Dirk van der Marel and Alexey Kuzmenko [37] employs Cryogenic Limited superconducting magnet of 7 T attached to a Vertex 70v Fourier transform spectrometer. This system allows reaching frequencies down to 8 cm^{-1} and temperatures lower than 10 K. For very low frequencies (1-100 cm^{-1}) a Time-Domain Spectrometer (TDS) coupled to a 4T superconducting magnet is available for reflective (transmission) measurements. The studied materials include topological insulators [38,39], graphene [40] and graphite [41].

The Infrared Laboratory from University of California, San-Diego, lead by Prof. Dimitri Basov [42] has a magneto-optical setup that is capable of broadband frequency domain spectroscopy in the range from 180 GHz to 750 THz at cryogenic temperatures [43]. The reflection unit of the setup couples both the Martin-Puplett and the Michelson interferometer to a 9 Tesla superconducting split coil magnet. Additionally the unit is designed to work with various detectors, including thermal bolometers and semiconducting detectors. The optical layout utilizes an intermediate focus while preserving optical f/#'s throughout enabling DC magnetic field measurements of small crystals with linearly polarized light in both Voigt and Faraday geometries. For transparent samples, simultaneous reflection and transmission can be performed. The

materials under investigation are high-Tc superconductors [44,45], topological insulators [46,47] and semiconductors with metal-insulator transitions [48].

The group of Dennis Drew [49] from University of Maryland developed magneto-optical setup with polarization modulation that allows measurements of the full complex Faraday angle, the rotation as well as the ellipticity, with an accuracy of 10 μrad/T [50,51]. The system operates on several far-infrared laser lines in the spectral range from 0.3 to 6 THz and utilizes optical split-coil magnet that allows obtaining results as a continuous function of temperature from 10 to 310 K and applied fields between ±8 T. The setup has permitted ground-breaking work in the study of multiferroics and electro-magnons [52,53], topological insulators [54,55,56], and high-*T*c cuprate superconductors [57,58].

The Solid State Spectroscopy group lead by Prof. Andrei Pimenov [59] at Vienna University of Technology developed a magneto-optical setup based on a Mach–Zehnder interferometer with a Backward Wave Oscillator (as a light source) coupled to a 8 T split-coil superconducting magnet with Mylar windows. The setup allows measurement of the complex (amplitude and phase) transmission and reflection coefficients in the THz spectral range ($4cm^{-1}$ - $40cm^{-1}$) as a function of external parameters like magnetic fields or temperature. Using Fresnel optical equations permittivity, conductivity or refractive index can be obtained without additional assumptions. The setup is used to reveal fundamental properties of condensed matter such as quantum Hall effect and charge dynamics in topological insulators [60,61,62], electron spin resonance in ferro- and antiferromagnetic media [63], magneto electric and magneto dielectric effect in

multiferroic materials linked to the so called electromagnons [64,65], energy gap, dynamics of the charge carriers, transversal and longitudinal resonances and quasiparticle relaxation rates in superconductors [66,67], negative refraction in metamaterials [68,69], etc.

To complete the review we cannot help mentioning the THz transmission and ellipsometry setups of Peter Armitage at Johns Hopkins U. [70,71,72,73] and magneto transmission-reflection setup of Ken Burch at Boston College. [74] All examples in this Section demonstrate that the field of magneto-optics using ellipsometry and polarimetry is rapidly developing in the recent years. The proposed here ellipsometry setup will be able to attract additional Users from the aforementioned Research groups to the new ellipsometry facility at MET, NSLS-II, BNL.

CHAPTER 3

FUNDAMENTALS of MM ELLIPSOMETRY and its APPLICATION to MULTIFERROICS

3.1 Basics of Bi-anisotropic Materials and Light Propagation in Bi-anisotropic Medium

Optical spectra of magneto-electric (ME) crystals are in the focus of modern experimental and theoretical studies [75,76,77,78,79,80,81,82,83,84,85,86,87,88,89, 90,91]. These materials can reveal a so-called *bi-anisotropic* optical behavior [92] in a form of the fascinating effects, such as colossal nonreciprocal light propagation [80,93,94,95], and a negative index of refraction [96,97]. These optical phenomena are expected to occur in resonance with electric and magnetic dipoles, for example, in the far-IR part of the optical spectrum, which is dominated by elementary excitations, such as optical phonons, magnons, electromagnons, and crystal field (CF) transitions. The common feature of all bi-anisotropic materials, and magneto-electric (ME) materials in particular, is that their optical properties cannot be correctly described with a dielectric susceptibility tensor $\hat{\varepsilon}(\omega)$ only. The magnetic permeability $\hat{\mu}(\omega)$ and ME tensors $\hat{\alpha}(\omega)$ and $\hat{\alpha}'(\omega)$ should be also included in consideration. As a result, a single transmission or reflection spectrum cannot properly describe the entangled contribution of $\hat{\varepsilon}(\omega)$, $\hat{\mu}(\omega)$, $\hat{\alpha}'(\omega)$, and $\hat{\alpha}(\omega)$ to, for example, the colossal nonreciprocal light propagation effect. ME coupling is a quintessence of bi-anisotropic optical effects. By

representing free energy *F* in terms of applied fields, where E and H are static fields or dynamic fields of light, the following expression can be written [98]:

$$-F(E,H)=\frac{1}{2}\varepsilon_0\varepsilon_{ij}E_iE_j+\frac{1}{2}\mu_0\mu_{ij}H_iH_j+\alpha_{ij}E_iH_j+\frac{1}{2}\beta_{ijk}E_iH_jH_k+\frac{1}{2}\gamma_{ijk}H_iE_jE_k+\ldots, \quad (3.1)$$

Where the first two terms in the right hand side represent conventional responses from electric and magnetic fields, $\hat{\alpha}$ describes the first order ME coupling. $\hat{\beta},\hat{\gamma}$ and further are high-order ME coupling tensors. To establish cross-terms for ME polarization $P_i(H_j)$ and ME magnetization $M_i(E_j)$, differentiation of F with respect to E_i and H_i results in:

$$P_i(H_j)=\alpha_{ij}H_j+\frac{1}{2}\beta_{ijk}H_jH_k+\ldots \quad \text{and} \quad \mu_0M_i(E_j)=\alpha^*_{ji}E_j+\frac{1}{2}\gamma_{ijk}E_jE_k+\ldots \quad (3.2)$$

Usually $\hat{\alpha}\neq 0$ requires certain magnetic point group symmetry with both conditions: no center of inversion and broken time-reverse invariance. The latter is always fulfilled in magnetically ordered states in the presence of spontaneous electric polarization.

The external magnetic field *H* changes all material tensors in Equations (3.1) and (3.2). The standard approach known from Landau-Lifshitz textbook is to modify the diagonal tensors ε and μ by adding imaginary terms $i\sigma H_z$ in the off-diagonal components,

which are proportional to the external field H ($\| z$) and quadratic-in-field corrections ($\delta \cdot H_z^2$) to the diagonal elements as follows:

$$\hat{\varepsilon} = \begin{bmatrix} \varepsilon_{xx} + \delta \cdot H_z^2 & -i\sigma \cdot H_z & 0 \\ i\sigma \cdot H_z & \varepsilon_{yy} + \delta \cdot H_z^2 & 0 \\ 0 & 0 & \varepsilon_{zz} \end{bmatrix}. \tag{3.3}$$

This conventional approach can describe phenomenologically a number of optical effects, such as Faraday rotation, but it is not complete. In a more general approach one should consider changes in the material's magnetic point group caused by external magnetic field and take into account all tensor components that are allowed by the new symmetry at $H \neq 0$.

The second term in the top line of Equation (3.2) is particularly interesting for this Project. If H_k is replaced with a strong external magnetic field H, then the β-term is not necessarily weak and can even overcome α (especially if α is small or even zero by symmetry). In Faraday configuration ($\vec{H} \| \vec{z}$), one can combine both terms together and introduce a new tensor $\rho_{ij}(H) = \alpha_{ij} + \beta_{ijk} H_k$ that will describe a generalized ME effect in external magnetic field, where α-term is for the natural ME component and the β-term is for effects caused by the external field. The constitutive relationship can be written as follows:

$$\begin{pmatrix} \vec{D} \\ \vec{B} \end{pmatrix} = \begin{pmatrix} \hat{\varepsilon} & \hat{\rho}(H) \\ \hat{\alpha}' & \hat{\mu} \end{pmatrix} \begin{pmatrix} \vec{E} \\ \vec{H} \end{pmatrix} \tag{3.4}$$

where ε and μ may have imaginary off-diagonal terms proportional to the field, like $\pm i\sigma H$ in Eq.(3.3), and $\rho_{ij}(H)$ has always some nonzero components in external fields due to the β-term. The challenge in the modelling of the light propagation described by Equation(3.4) is that $\hat{\rho}$ and $\hat{\alpha}'$ are no longer transpose-complex-conjugate to each other, as one always expects at $H = 0$, when one expects $\hat{\alpha}' = \hat{\alpha}^{\dagger}$ [99].

The most interesting experimental situation could be realized in a material with $\hat{\alpha} = 0$ at low fields, which is close to criticality and, hence, becomes ME ($\hat{\alpha} \neq 0$) above a certain magnetic field H_C. For example, this situation is realized in antiferromagnetic materials in the vicinity of a second-order spin-flop transition as in Ni_3TeO_6. [100] In the low-temperature antiferromagnetic phase the presence of a translation by half a unit cell combined with time-reversal is present in the symmetry group, therefore the ME effect is forbidden. In the spin-flopped phase at high field H this symmetry is broken, and ME effect is allowed: $\hat{\alpha} \neq 0$. Sensitive dependence of the ME constant on the changing magnetic structure is encoded in the terms with β_{ijk} and of higher orders in the fields. This situation is experimentally accessible, and results to some of the largest ME effects observed so far. In the systems where the transition is weakly first order, the domain wall motion gives rise to the ME constant. Optical measurements are essential to distinguish between the intrinsic and the domain wall contributions, as they allow to measure the frequency dependence of the ME tensor.

Instead of conventional transmission or reflection optical measurements of ME materials, here we propose a combination of a significantly more advanced spectroscopic

technique together with an adequate theoretical description. The proposed Mueller matrix spectroscopic ellipsometry (MM-SE) is an ideal and probably the only method to study fundamental properties of the generalized ME tensor $\rho_{ij}(H) = \alpha_{ij} + \beta_{ijk} H_k$ and its influence on the light propagation in bi-anisotropic media. On the theory side, the group of Prof. Sirenko at NJIT has already developed models and simulation tools for analysis of the Mueller matrices (MM) for experimental optical spectra using the 4×4 Berreman's matrix formalism. Prof. Sirenko's group has found that the off-diagonal components of the MM spectra at *H*=0 are proportional to $\hat{\alpha}(\omega)$ and $\hat{\alpha}'(\omega)$, while the contributions of $\hat{\varepsilon}(\omega)$ and $\hat{\mu}(\omega)$ have opposite sign in the diagonal MM components, thus providing a direct experimental method of separation $\hat{\varepsilon}(\omega)$, $\hat{\mu}(\omega)$, $\hat{\alpha}(\omega)$, and $\hat{\alpha}'(\omega)$.[8] The future theoretical extension of the theoretical methods will be an addition of $\pm i\sigma H$ and $\rho_{ij}(\omega, H) = \alpha_{ij}(\omega) + \beta_{ijk}(\omega) \cdot H_k$ terms in the simulation tools. Since MMs have 8 independent off-diagonal spectra that include contributions from $\pm i\sigma H$, $\hat{\alpha}'$ and $\hat{\rho}(H)$, one should be able to separate their contributions to the classical Faraday effect and possible non-reciprocal light propagation. Note that in conventional transmission/reflection spectra the contributions from $\pm i\sigma(\omega)H$ and $\rho(\omega, H)$ terms are indistinguishable due to degeneracy of the *s*- and *p*-polarized light at the normal incidence. In contrast, in a full MM analysis, these tensors contribute to different off-diagonal MM spectra and can be separated, especially in experiments using variable external field applied in both, Faraday and Voigt configurations.

3.2 METHOD: Combination of MM-SE and 4×4 Berreman's Simulation Approach

Realization of the proposed design will allow Users of MET to challenge the present state of the art in polarization analysis for the spectra of magnetic, electric, and electromagnon excitations in ME and bi-anisotropic materials. In the most known to us publications on the far-IR spectra in multiferroics, the polarization analysis of magnons, electromagnons, and phonons has been always restricted by the experimental geometry with the near-to-normal angle of incidence (AOI) and by the use of linear polarizers only. Using 4×4 Berreman's matrix propagation approach, one can easily show that the normal incidence geometry is *not* always sensitive to the dynamic ME effects described by the $\hat{\alpha}(\omega)$ and $\hat{\alpha}'(\omega)$ tensors. A simultaneous presence of the *s*- and *p*-polarizations is required to have complete information about the optical properties of a ME material. At AOI=0, the *s*- and *p*-polarizations are obviously degenerate. Thus, the traditional approach to analysis of dynamic polarization in ME media at AOI=0 is incomplete. For example, the limitations of the AOI=0 geometry recently revealed themselves by failing to explain the experimentally-observed suppression of electromagnons in reflectivity measurements of $GdMnO_3$ [101]. As an alternative, a more advanced method is required. This method is a combination of new experimental and computational techniques using AOI≠0: (i) MM-SE at MET beamline NSLS-II, BNL and (ii) advanced data analysis and simulation approach for the MM spectra based on the Berreman's 4×4 matrix propagation technique [4,5,8,15].

3.3 Basics of the Muller Matrix Spectroscopic Ellipsometry (MM-SE)

Spectroscopic Ellipsometry measures changes of the light polarization upon reflection from a sample in a wide frequency range. [102,103,104,105,106,107,108,109,110, 111, 112,113,114,115] MM-SE tools are commonly available for mid-IR –VIS parts of the spectrum in many fields, from Telecom and Quantum Cryptography to Biology and, finally, Condensed Matter Physics [116]. In spite of the power of the MM-SE technique, no *commercial* MM-SE are available for the far-IR/THz range. Prof Sirenko, NJIT and his co-workers built the first instrument in 2010 at U4IR beamline at NSLS-BNL.[8] The main challenge was the lack of the optical components, such as optical retarders, for the far-IR spectral range. This issue has been successfully solved by using plastic, KRS5, ZnSe, and Si retarders to produce a broadband circularly polarized light in THz and far-IR [5].

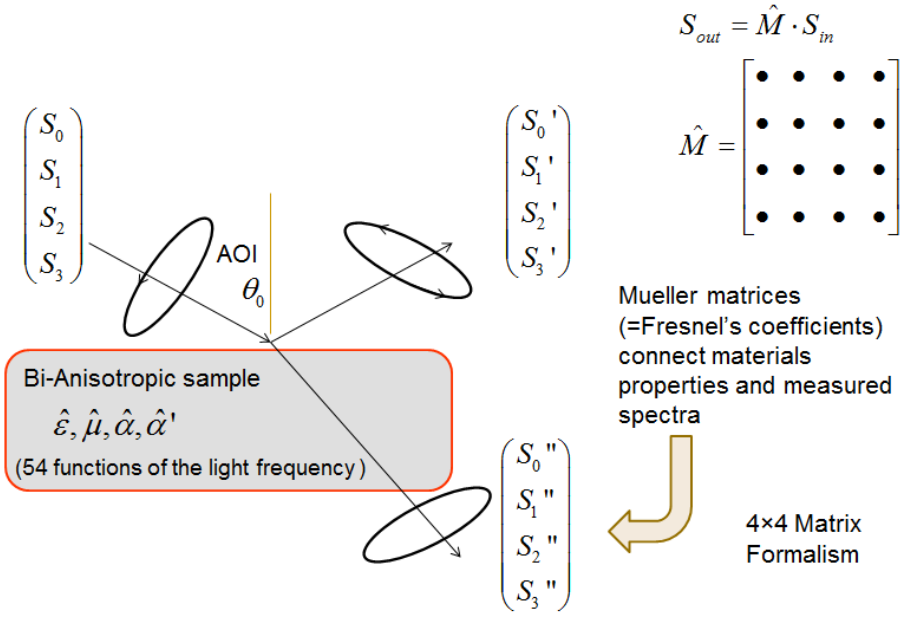

Figure 3.1 Schematics for MM-SE experiments. The polarization of the reflected light is described using Stokes-vector representation.

The MM formalism is based on the Stokes vector representation for the light polarization [109], where the real components of the Stokes vectors for the input $\vec{S}_{IN}$ and output $\vec{S}_{OUT}$ light are connected with the 4×4 Muller matrix $\hat{M}$ of the sample: $\vec{S}_{OUT} = \hat{M} \cdot \vec{S}_{IN}$. In the Stokes representation, the polarization vectors for liner and circularly polarized light are $S_1 = (1, \pm1, 0, 0)$, $S_2 = (1, 0, \pm1, 0)$, and $S_3 = (1, 0, 0, \pm1)$. The 16 components of $\hat{M}$ are real functions of the complex Fresnel coefficients and the conversion between complex 2×2 Jones and real 4×4 MM's, $r_{s,p,sp,ps} \Rightarrow M_{ij}$ is straightforward in the absence of random scattering as described in Reference [117]. To compensate for both, the spectral variation of the incoming radiation and for the spectral response of the experimental setup, the MM components $M_{ij}(\omega)$ are usually replaced by the normalized ones $m_{ij}(\omega)$, where $m_{ij} = M_{ij} / M_{11}$ and M_{11} is the total reflectivity. Thus, MM-SE can generate 15 normalized components of the MM spectra $\hat{m}(\omega)$ which contain significantly more information about anisotropic, magnetic, and ME samples compared to that for transmission/reflection experiments at AOI=0, when *s*- and *p*-polarized light is degenerate. The theory of operations for MM-SE, which have been previously implemented at U4-IR setup, is published in Reference [8].

Theory of Operations:

- Polarization measurements of the MM components $m_{ij}(\omega, \theta)$ at several AOIs in the range between 70 and 80 deg and correction for the systematic errors of experiment, such as non-ideal polarizers, retarders, windows, *etc*.

- Sample modeling using, a parametric description for the dielectric $\hat{\varepsilon}(\omega)$, magnetic $\hat{\mu}(\omega)$, and ME $\hat{\alpha}(\omega)$ and $\hat{\alpha}'(\omega)$ tensors and application of the 4×4 Berreman's matrix propagation approach to calculate the MM spectra $m_{ij}(\omega,\theta)$, or solving a "direct problem": $\{\hat{\varepsilon}(\omega),\hat{\mu}(\omega),\hat{\alpha}(\omega),\hat{\alpha}'(\omega),\theta\}^{[3\times3]} \Rightarrow m_{ij}(\omega,\theta)^{[4\times4]}$.
- Solving the "inverse problem" to determine the model input parameters, such as the oscillator frequencies ω_0, broadening γ, and strength of electric, magnetic, and ME dipoles $S_{e,m,ME}$, that provide the best match between experimental and modeled spectra: $m_{ij}(\omega,\theta)^{[4\times4]} \Rightarrow \sum \omega_0, S_{e,m,ME}, \gamma, \ldots$. The fitting Program for MM spectra has been developed in Prof. Sirenko's Group and is available to all Users of the MM-SE setup. The primary spectral range of our MM-SE at is between ~20 and 4,000 cm^{-1}. The low-frequency cut off is determined by diffraction and, correspondingly, can be shifted down to ~10 cm^{-1} for big crystals larger than 25 mm^2 or shifted up to ~30 cm^{-1} for small samples with the size of a few mm^2. Thus, the spectral range for almost all known magnetic excitations (magnons, electromagnons) and IR-active optical phonons in magnetic oxides can be covered.

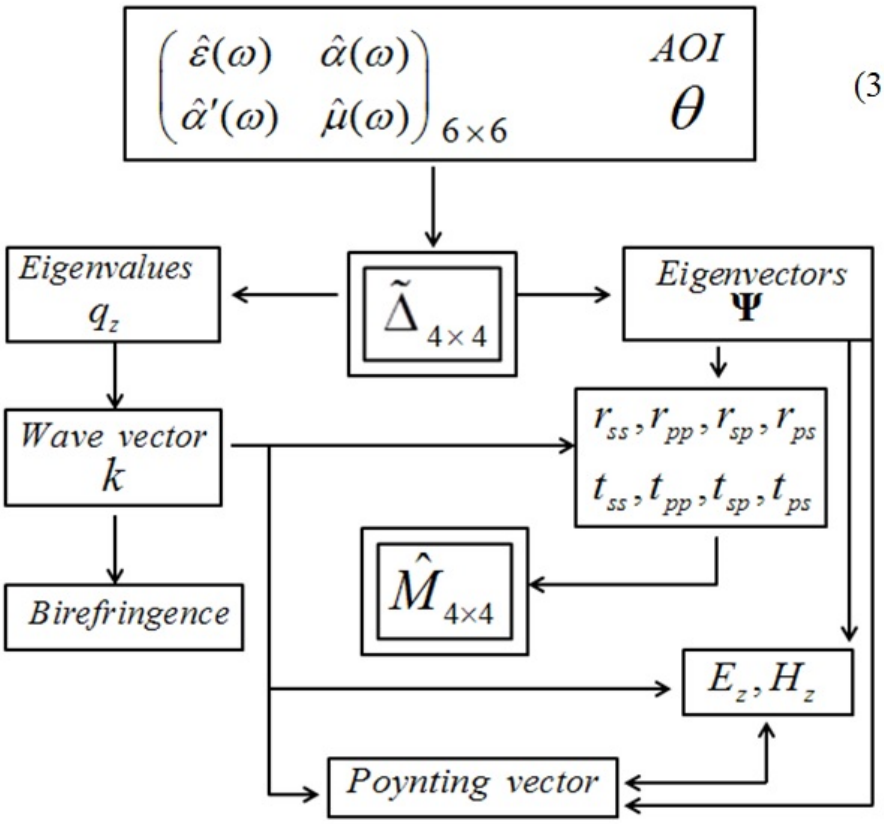

(3.5)

Figure 3.2 Flowchart for the MM calculation steps in Berreman's 4×4 matrix formalism [15].

3.4 Berreman's 4x4 Matrix Propagation Technique for Optical Spectra Analysis

A proper analysis of the light propagation in ME and multiferroic materials in the far-IR frequency ranges and low temperatures when all elementary excitations (magnons, electromagnons, phonons, and 4*f* electronic CF transitions) are optically active, is based on the following set of the medium's constitutive relations described by Equation (3.4). The 4×4 matrix formalism, as developed by Berreman [118], which provides for an accurate and systematic method of obtaining numerical, and in some cases, analytic solutions for electromagnetic wave propagation in bi-anisotropic medium:

$$\begin{pmatrix} 0 & -curl \\ curl & 0 \end{pmatrix}\begin{pmatrix} \vec{E} \\ \vec{H} \end{pmatrix} = i\frac{\omega}{c}\begin{pmatrix} \hat{\varepsilon} & \hat{\alpha} \\ \hat{\alpha}' & \hat{\mu} \end{pmatrix}\begin{pmatrix} \vec{E} \\ \vec{H} \end{pmatrix} \tag{3.6}$$

In the right-hand-side of Eq. (3.6), the 6×6 big optical matrix, which includes all anisotropic tensors $\hat{\varepsilon}(\omega)$, $\hat{\mu}(\omega)$, $\hat{\alpha}(\omega)$ and $\hat{\alpha}'(\omega)$. Equation (3.6) can be reduced to the Berreman's equation: [118,119]:

$$d\vec{\Psi}/dz = i(\omega/c)\tilde{\Delta}\vec{\Psi} \ . \tag{3.7}$$

$\vec{\Psi}$ is an array of the transverse components of the electromagnetic wave $\vec{\Psi} = [E_x, H_y, E_y, -H_x]^T$ in the medium and is an eigenvector of $\tilde{\Delta}$, where $\tilde{\Delta}$ is a 4×4 matrix constructed from the same set of components of the $\hat{\varepsilon}$, $\hat{\mu}$, $\hat{\alpha}$ and $\hat{\alpha}'$ tensors as the 6×6 optical matrix in Equation (3.6), see also Figure 3.2. The eigenvalues and eigenvector solutions to the Berreman equation represent wave vectors and the transverse components of the propagating electromagnetic waves, respectively. These solutions are unique to the

crystal symmetries and constitutive relations incorporated into the $\tilde{\Lambda}$ matrix. Figure 3.2 shows the flowchart for 4×4 formalism calculations, which is described in details in Refs. [8]. In principle, all components of the MM are functions of all components of the electric, magnetic, and magneto-electric tensors: $m_{ij}(\omega,\theta) = f\left(\varepsilon_{ij}(\omega), \mu_{ij}(\omega), \alpha_{ij}(\omega), \alpha'_{ij}(\omega)\right)$. But in the case of a relatively high point group symmetry, like in hexagonal crystals, the close-to-diagonal components of the MM $m_{12,22,21,33,34,43,44}(\omega,\theta)$ depend mostly on $\varepsilon_{ij}(\omega)$ and $\mu_{ij}(\omega)$, while the off-diagonal components of the MM, such as $m_{13,14,23,24,31,32,41,42}(\omega,\theta)$ depend only on $\alpha_{ij}(\omega)$ and $\alpha'_{ij}(\omega)$. It is also very important observation that the contribution of $\varepsilon_{ij}(\omega)$ and $\mu_{ij}(\omega)$ components have an opposite sign in, for example, $m_{43}(\omega,\theta)$ spectra. Figure 3.3 illustrates this great potential of the combination of the MM-SE technique and the Berreman's 4×4 propagation matrix formalism for analysis of magnetic materials. We present here our published data for recent MM-SE measurements in $Dy_3Fe_5O_{12}$ iron garnet (Dy-IG), where magnetic and electric dipoles at 59.5 and 81.5 cm^{-1} have been experimentally identified, spectrally separated, and their parameters have been determined from a single MM measurement without adducing any additional arguments about their strength, frequency, or temperature dependence. [8] This capability of MM-SE is conceptually similar to a widely known fact that conventional Ellipsometry can directly measure real and imaginary parts of $\varepsilon(\omega)$ without using Kramers-Kronig transformation.

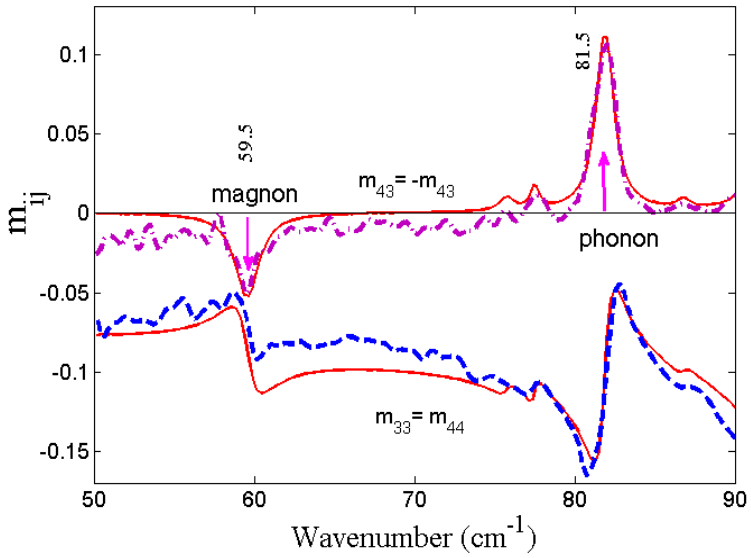

Figure 3.3 (From Reference [8]) Experimental spectra of the normalized MM components $m_{43}(\omega) = -m_{34}(\omega)$ (magenta dot-dash curve) and $m_{33}(\omega) = m_{44}(\omega)$ (blue dash curve) for Dy-IG measured at T = 5 K. The peak at 81.5 cm^{-1} correspond to the optical phonon, the peak at 59.5 cm^{-1} is a magnon. Solid red curves show the fit results based on the Berreman's 4×4 propagation matrix formalism. Note that both, the experiment and model prediction show that the magnon amplitude in the $m_{43}(\omega) = -m_{34}(\omega)$ spectra has an opposite sign compared to that for the phonon as indicated by pink arrows.

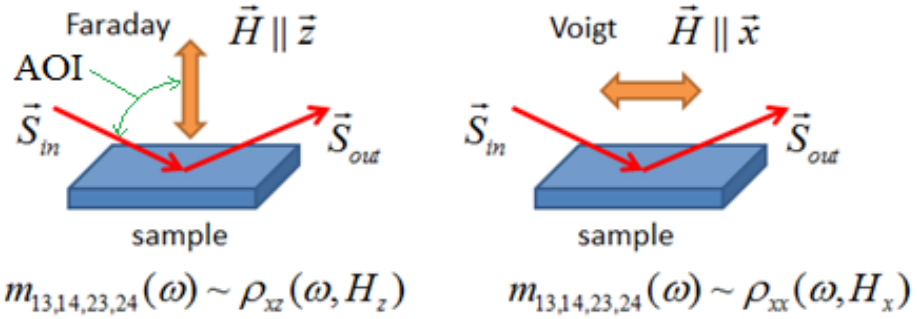

Figure 3.4 Above figure illustrate the Faraday and Voigt configurations. Red arrows show IR light with polarization described with the Stokes vectors $\vec{S}_{in}$ and $\vec{S}_{out}$. Thick double-head arrow shows the external magnetic field direction.

3.5 Importance of using both Faraday and Voigt Field Configurations in the Same Experimental Setup

In the opto-mechanical design layout of this instrument the orientations of the external magnetic field in the sample plane (Voigt) and perpendicular to the sample surface (Faraday) are given equally importance and considerations. When field is in the plane of the sample, the main measurable effect in the spectra of the off-diagonal components of the MM $m(\omega)$ is expected to be induced by the *diagonal* components of the generalized ME tensor $\hat{\rho}(H)$, where $\rho_{xx}(H) \| H_x$. In contrast, in the Faraday configuration the dominant contribution to the MM spectra should appear from the *off-diagonal* components of the $\hat{\rho}(H)$ tensor: $\rho_{xx}(H) \| H_x$. By choosing two different orientations of the field for the same bulk crystal, we should be able to measure the entire $\hat{\rho}(H)$ tensor and, hopefully, separate the ME tensor components from the linear terms $\pm i\sigma H$ in the $\hat{\varepsilon}$ tensor. Figure 3.4 illustrates the Faraday and Voigt configurations and the effect of the magnetic field on components of the $\hat{\rho}(H)$ tensor.

3.6 Recent Accomplishments in MM-SE using far-IR Synchrotron Radiation

Using MM-SE at the U4IR beamline of NSLS-BNL the research group of Prof. Sirenko measured recently ME components of the electromagnon spectrum in $TbMnO_3$. The unique advantage of MM-SE for studies of dynamic ME effects in multiferroics is illustrated in Figure 3.5. An *experimental decoupling* of the electromagnon components in $\hat{\varepsilon}(\omega)$, $\hat{\mu}(\omega)$, $\hat{\alpha}(\omega)$ and $\hat{\alpha}'(\omega)$ tensors has be done in a single measurement cycle. Pink arrows in Figure 3.5(b) show the contribution from $\varepsilon_{xx}(x \parallel a)$ and $\mu_{yy}(y \parallel c)$ to the measured $m_{43}(\omega)$ spectra. The experimental spectra of the electromagnon in

$m_{14,24}(\omega)$, $m_{33,44}(\omega)$, and $m_{34,43}(\omega)$ allow to determine the oscillator strength $S_{xx}^{e} = 1.6 \pm 0.2$ and $S_{xz}^{EM} = 0.2 \pm 0.05$ of the electromagnon in $\varepsilon_{xx}(\omega)$, and $\alpha_{xz}(\omega)$ at 62 cm^{-1}. In turn, the latter parameters are directly related to the static electric polarization of the lattice due to the spin structure $\vec{P}_S$, and anisotropy and exchange fields for the spin structure.

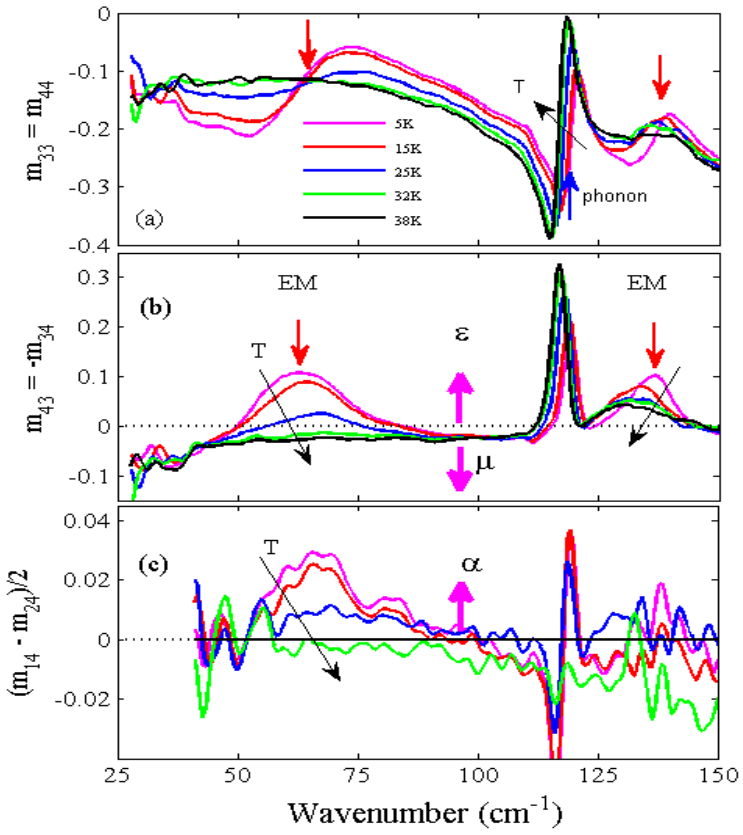

Figure 3.5 Experimental spectra of $TbMnO_3$ with x‖a, y‖a, and z‖b measured in the temperature range between 5 K and 40 K. Phonon peak at ~118.5 cm^{-1} and two electromagnon peaks (EM) at 62 and 135 cm^{-1} are marked with red arrows. The MM components are shown in (a) $m_{33}(\omega) = m_{44}(\omega)$ and (b) $m_{43}(\omega) = -m_{34}(\omega)$. (c) The difference between the off-diagonal MM components $m_{14}(\omega)$ and $m_{24}(\omega)$. Pink arrows in (b) and (c) indicate the sign of the theoretical contribution of $\varepsilon_{xx}(\omega)$, $\mu_{yy}(\omega)$, and $\alpha_{xz}(\omega)$ to the MM components. From Reference [8].

CHAPTER 4

DESIGN of OPTO-MECHANICAL DESIGN of SYNCHROTRON RADIATION-BASED FAR-INFRARED SPECTROSCOPIC ELLIPSOMETER WITH STRONG MAGNETIC-FIELD

4.1 Components and Technical Details for SR-MM-SE

This Chapter presents the original results for the Theses. Several components of the instrument design, mechanical solutions, magnetic field solutions, vacuum solutions, sample low temperature cooling, and optics solutions will be discussed in detail. Figure 4.1 shows the general setup of the ellipsometer. The ellipsometer is made up of five main components,

- PSG chamber
- Gate valves and bellow connections to the sample chamber
- magnet
- Sample load chamber and
- PSA chamber

These instrument chambers are detachable from one another. They are coupled using flexible bellows. PSA and Sample load chambers are mounted on rotational stages and they could be arranged in configurations suitable to for the experimental geometry. Below the design will be described.

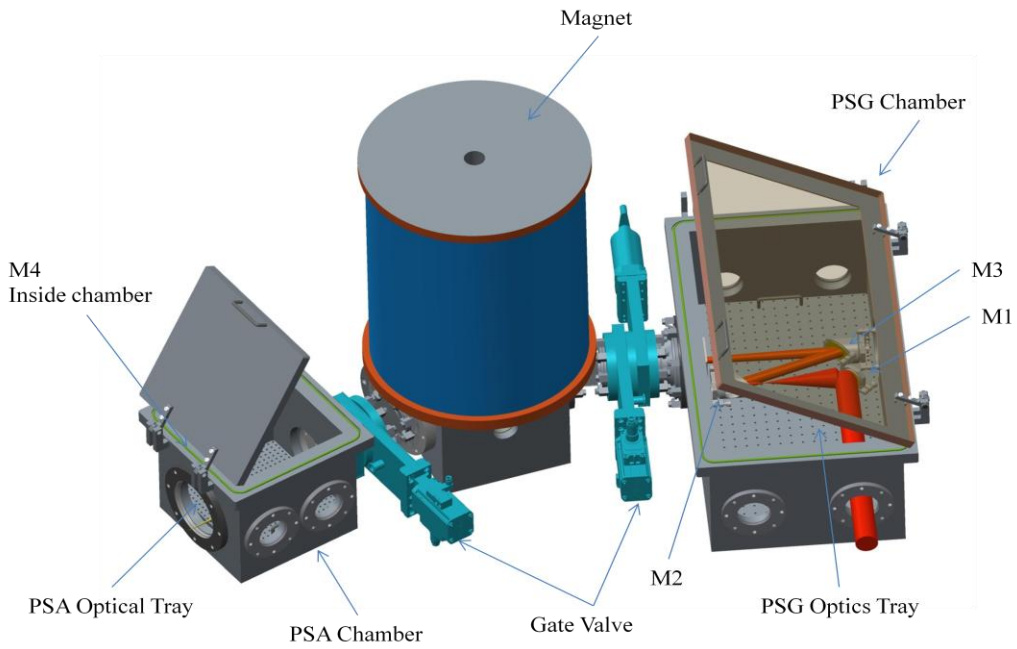

Figure 4.1 3D view of the ellipsometer at MET beamline which consists of four major parts: a 9 T magnet in the center, Polarization State Generation (PSG) section, Gate Valves Connections, and Polarization State Analyzer (PSA) section.

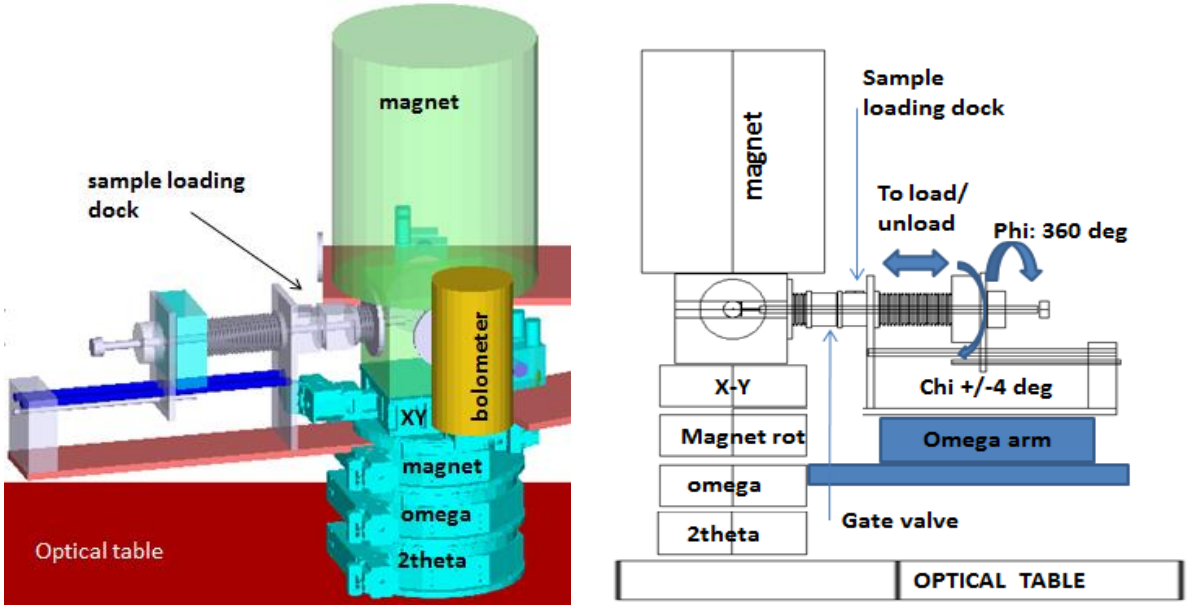

(a) (b)

Figure 4.2 (a) 3D view of the sample chamber and the magnet for the ellipsometer at MET beamline: a 9 T magnet in the center, and side-load cold finger Sample Stage. The magnet is supported by the rotational stage to enable the change of AOI, a switch between Voigt and Faraday configurations, and sample alignment. (b) A side view cross section shows the sample load section and sample alignment in *Omega*, *Chi*, and *Phi* directions.

4.2 Mechanical Solutions

Our proposed mechanical design allows for AOI variation between 70 and 85 deg, sample alignment in both *Chi* and *Omega* directions by +/- 4 deg, and *Phi* rotation of anisotropic samples by 90 deg around Z axis, as shown in Fig. 4.2(b).

Ellipsometry is one of the most sensitive optical techniques. Its outstanding capabilities in determination of the sample dielectric properties depend on the mechanical

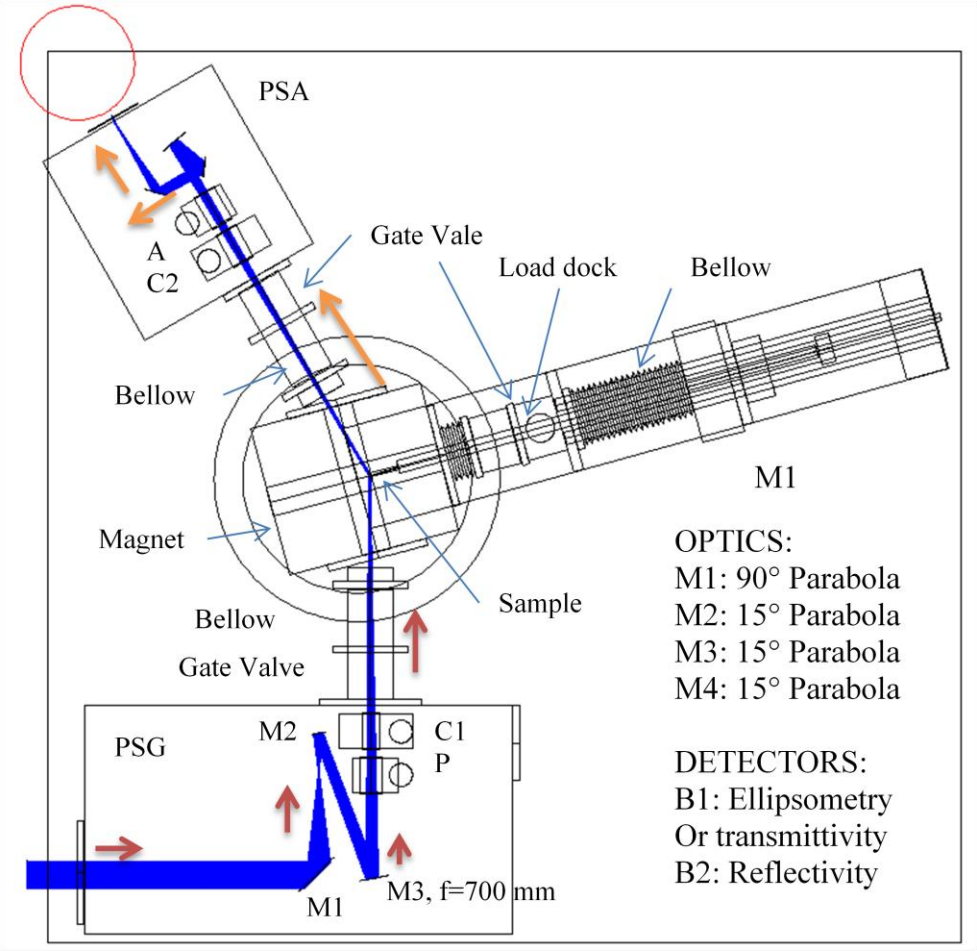

Figure 4.3 ZEMAX simulation of the light propagation (blue color) inside the ellipsometer (top view). The magnet, the Sample Stage and PSA section can rotate around the same vertical axis to accommodate the ellipsometry measurements at different AOIs.

stability against vibrations, and reproducibility of the sample and polarizers positions during the measurements. The low-temperature and strong magnetic field aspects require a careful choice of all mechanical components. The central part of the mechanical setup is the HUBER 3-circle coaxial assembly consisting of the *magnet XY table*, *omega arm*, and *2-theta arm* [see Figure 4.2(a)]. This assembly is capable to carry the total weight load of up to 600 kg, thus exceeding at least three times the projected weight of the magnet (~200 kg). The mechanical design can provide an angular accuracy of about 0.01 deg that is typical for high-resolution x-ray diffraction experiments. In the following description we use the axes notation adopted in both ellipsometry and x-ray community, such as *Omega*, *2Theta*, *Chi*, and *Phi*. For *XYZ* directions we use the ellipsometry notation where *Z* is perpendicular to the sample surface, *X* is along the light reflection plane, and *Y* is perpendicular to the reflection plane.

The *magnet table* provides a capability to adjust the magnet position by several degrees for the ellipsometry measurements with variable AOIs within a range between 70 and 85 deg. This stage will also allow for the magnet rotation by 90 deg when orientation of the field is switched between Faraday and Voigt configurations. And finally, this mechanical circle will allow Users to switch between Ellipsometry at glancing AOI and classical Transmission/Reflection configurations for AOI=0. The linear translation stage will allow for a quick repositioning of the magnet by +/- 25 mm to adjust for the difference between the sample position and the vertical axis of the magnet bore.

The *Omega arm* is design to hold the sample on the cold finger of the LHe-flow cryostat. In the ellisometry measurements the main role of the *Omega arm* is to enable the sample alignment. The inner diameter of the magnet horizontal bore allows for the sample adjustment in the range of +/- 4 deg for *Omega* direction. This adjustment range is sufficient for a typical experimental situation that requires alignment of a small sample mounted on a cold finger. The *Omega arm* also supports the *Chi* stage, which provides the corresponding adjustment of the sample position of +/- 4 deg for *Chi* direction (orthogonal to *Omega*). The center of rotation for the *Chi* stage is at the sample surface inside the magnet. The *Phi* stage, which is positioned at the center of the *Chi* stage, will provide a possibility to rotate the sample 90 deg around the *Z* axis. This rotation is possible even for a cold sample in the measurement position. The *Omega arm* is also holding the sample quick reload section, which consists of the loading dock separated from the magnet volume by a gate valve. The long translation stage allows for bringing the sample in the measurement position inside the magnet and for retrieving the sample through the gate of the loading dock. The sample exchange time is quick: it will consist of the main intervals of ~30 min for warming up to 300 K, physical exchange of the sample pegs on the cold finger (~30 min), and pumping the sample volume down to the cryogenic pressure of 10^{-6} Torr (~ 1 hour).

The *2-Theta* arm is holding the PSA section and bolometer / IR detector. The main purpose of this arm is to compensate for the sample alignment using *Omega* arm and to provide a capability to measure ellipsometry data at variable AOIs. This arm also

allows for an “alignment-free” conversion of the setup between Ellipsometry and conventional see-through Transmission geometries.

PSG (Polarization State Generation) Chamber

The Polarization State Generation (PSG) Chamber is connected to the 9 T spectromag sample chamber with ISO flanges, bellows and gate valves. The PSG chamber is designed to support all optics on top of a removable optical tray. The PSG chambers is robustly constructed with aluminum thick walls welded in to box that ensures it is capable of holding high vacuum volumes and providing mechanical stability. The reproducibility of the sample dielectric properties depends on the mechanical stability against vibrations and polarizers position during the measurements. The design of this PSG chamber is stable enough that the chamber will hold 10^{-3} Tor vacuum when in operating condition. The PSG chamber is made of Aluminum 6061-T6, and 20 mm thick walls. The chamber is 324 high x 438 wide x 788 mm long. The 2D drawings are shown in Appendix.

The PSG chamber is made with ISO flanges for quick and essay connections to other components, such as spectro-mag sample holding chamber, see Figures 4.3 and 4.4. The ISO flange for the main optical axis connecting to the sample chamber is ISO-160. The ISO-80 flanges provide connections to attach the bolometer, marked as B2 detector in Figure 4.3. There are four ISO-80 flanges available, two on each side such that synchrotron radiation source or detector could be connected to the instrument at any of the given optical configuration. Other unused ISO-80 or ISO-160 connections could be

blocked with a blank ISO-Caps. Each ISO-Cap is a standard blank plate with seal, therefore, chamber is fully sealed and vacuum retention could be maintained as needed. The blank ISO caps hold electrical feedthroughs for motors inside the vacuum chambers.

The PSG chamber is made with detachable lid. The lid itself is attached to the box with hinges. This hinge is designed such that when desired it could be detached from the PSG chamber box by removing the pin, see Figure 4.5. The hinge connecting pin is kept in place with two spiral retaining rings. In order to detach the chamber lid one can remove the hinge connection pin by removing the spiral retaining ring. See Figure 4.4 for a detail view.

The lid sits on the chamber box on a gasket to seal the chamber. The seal ensures vacuum volume retention during the operation of the experiment. The groove for the seal is in the chamber box so that when vacuum is being drawn from the chamber the seal keeps itself in place and not suck down into the chamber. The lid is made with two handles such that when desired the lid could be easily opened and closed. See Figure 4.3.

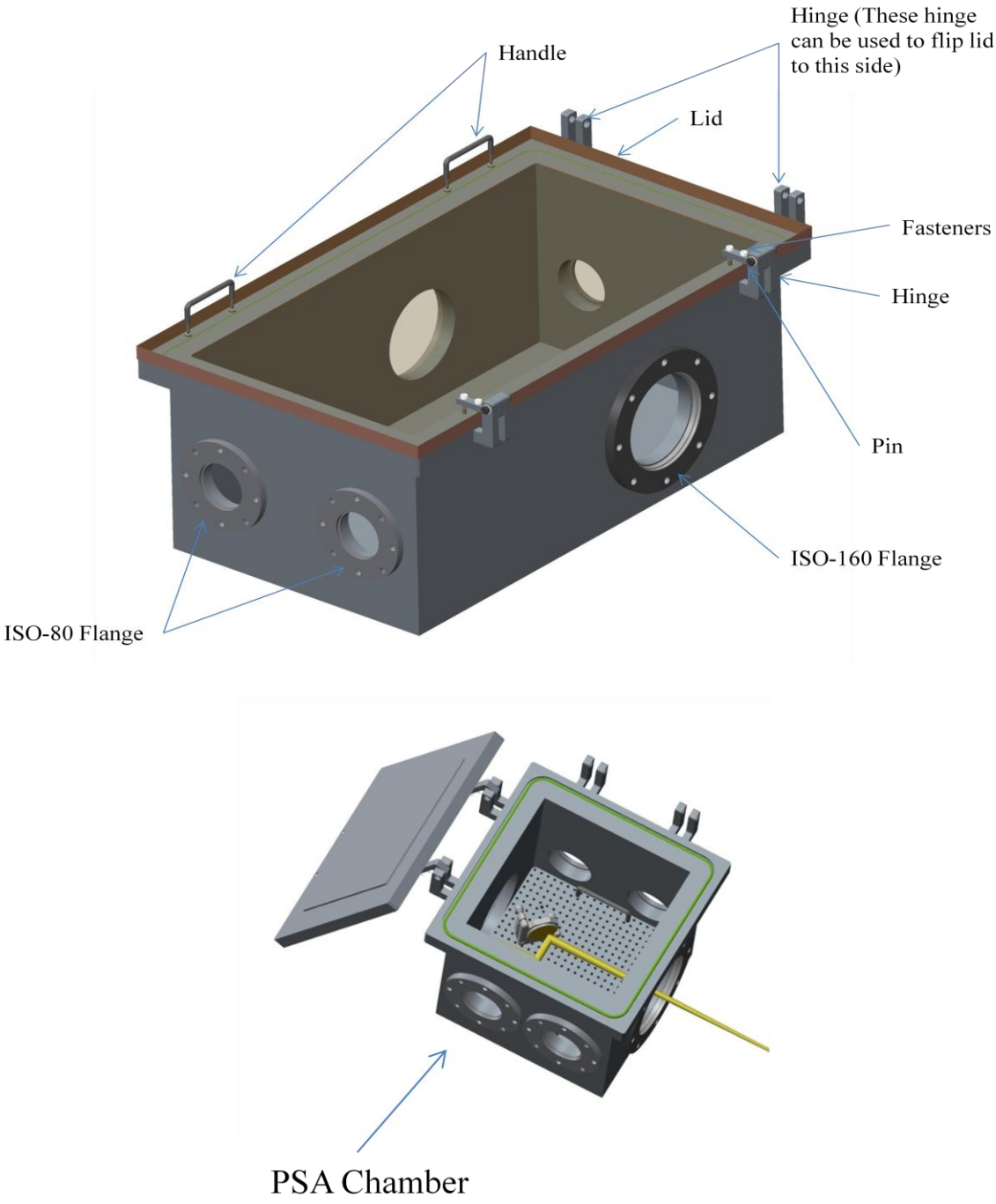

Figure 4.4 (Polarization State Generation (PSG) chamber (top) and Polarization State Analyzer (PSA) chamber (bottom) are shown in in 3-D view with removable lid. The lid could also be flipped to the other-side by using additional available hinges.

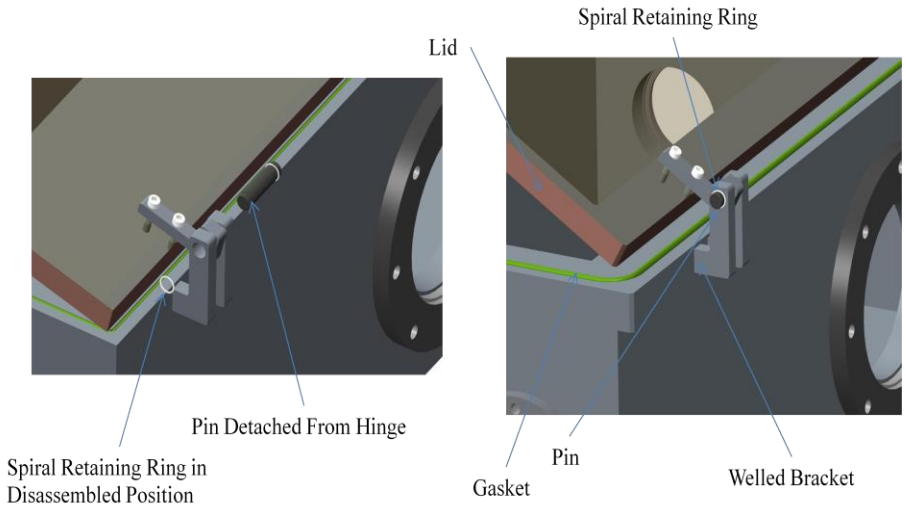

Figure 4.5 Hinge mechanism assembly and disassembly. The lid could be detached upon the removal of the pin.

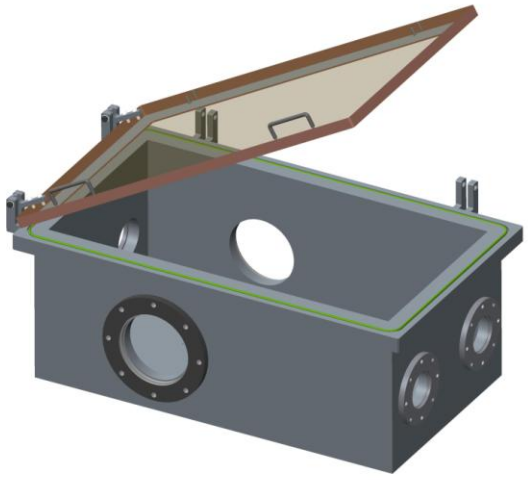

Figure 4.6 Polarization State Generation (PSG) chamber is shown in another configuration where user can open the lid on the lefthand side.

PSA (Polarization State Analyzer) Chamber

The Polarization State Analyzer (PSA) Chamber is connected to the 9 T spectromag sample chamber with ISO flanges, bellows and gate valves. The chamber is designed to support all optics on top of a removable optical tray similar to the PSG Chamber. The PSA chambers is robustly constructed with aluminum thick walls welded in to box that ensures robust construction that is capable of holding high vacuum and providing

mechanical stability. The reproducibility of the sample dielectric properties depends on the mechanical stability against vibrations and polarizers position during the measurements. The design of this PSA chamber is stable enough that the chamber will hold 10^{-3} Tor vacuum when in operating condition. The PSA chamber is made of Aluminum 6061-T6 with 20 mm thick walls. The chamber is 324 high x 320 wide x 320 mm long as shown in Figure 4.3 (bottom). The 2D drawings are shown in Appendix.

Gate Valves and Bellow Connection

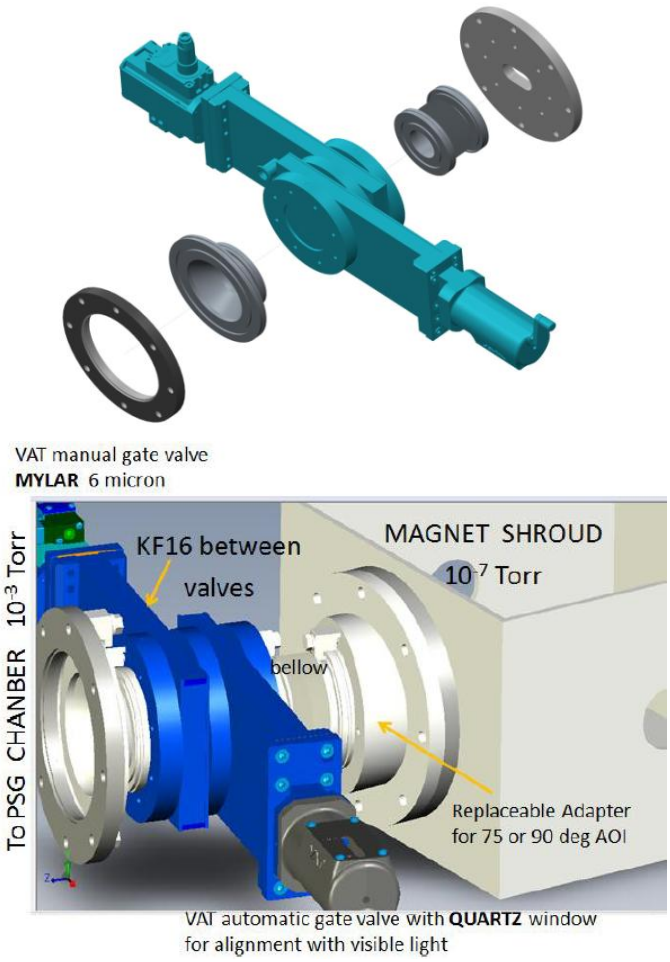

Figure 4.7 The cross-section shows polarizer and retarder holder, conical reducer adopter, and two gate valves.

The Polarization State Generation (PSG) chamber ISO-160 flange connects to conical reducer adopter. This reducer adapter has ISO-160 connection to the PSG chamber side and ISO-80 to the gate valve side. This conical reducer is made such that it accommodates a retarder inside. This type of configuration saves space and reduces the overall foot print of PSG. The conical reducer connects to a pair of VAT gate valves (see Figure 4.7). One gate valve is automatic (solenoid-operated) and the second one is manually (mechanically) operated. Mechanical gate valve holds a 6 micron mylar window. The automatic valve is equipped with a hard window. The purpose of such combination is explained in more details in the *Vacuum Solutions* Section. The last component connecting the VAT gate valves to the center sampler holder chamber with a flexible bellow with ISO-80 flanges at each end. This flexible component makes up for any mechanical misalignment while the optical axis are kept in position, see figure 4.7. Each of the end ISO-160 connections are secured with claw clamps.

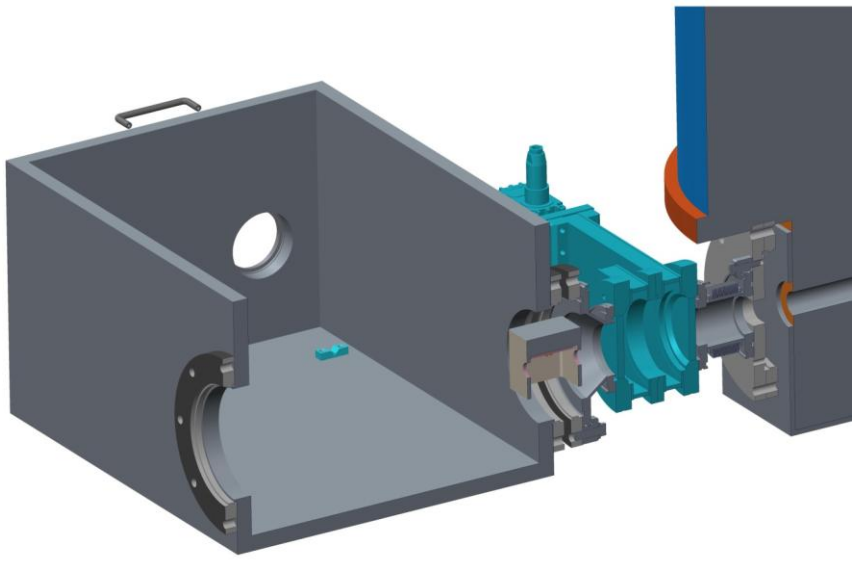

Figure 4.8 The cross-section shows polarizer and retarder holder, conical reducer adopter, and two gate valves.

Optical Tray Mount

The PSG chamber is made with four holes in at the bottom of the chamber (see appendix drawing). These holes allow for four precision dowel pins for the optical tray. Each one of the four pin are situated to hold and lock X-Y optical axis for the optical tray see Figure 4.9.

The optical tray is designed to have four kinematic bases standoff legs. These legs are mounted to the optical tray assembly with screws. Each leg is 1 inch tall, aligning the optical tray height at z-axis with the ellipsometer sample holder. The Kinematic mount system is designed to create a stable platform for the optical tray. These standoff legs ensure stable positioning of the optical tray each time user placing it in the chamber or outside the chamber on any table for optical alignment. The standoff legs have hole in the center to receive the dowel pins positioned in the chamber bottom plate. This pin aligning system is designed so user could have accurate repeatability of the optical alignment with the instrument optics each time when the optical tray is placed inside the chamber (see figure 4.9).

PSG and PSA Optical Tray

The optical tray is designed to be removable from the chamber. This type of setup allows the user to setup optics on an optical table outside of the instrument. At the same time, the possible deformations of the PSA and PSG chambers caused by vacuum are decoupled from optics. The design provides Users with multiple options for optical layout, easier alignment of optics and open space to work in. The tray is made of ¼”

think aluminum 6061-T6 plate with standard imperial breadboard hole patterns. The tray has two handles, one on each side for stable carry and pickup. See Figure 4.9 and 4.10. The Optical tray has standard 1 [in] x 1[in] hole pattern to hold any optical systems posts or optics. The PSG and PSA optical tray are similar is design.

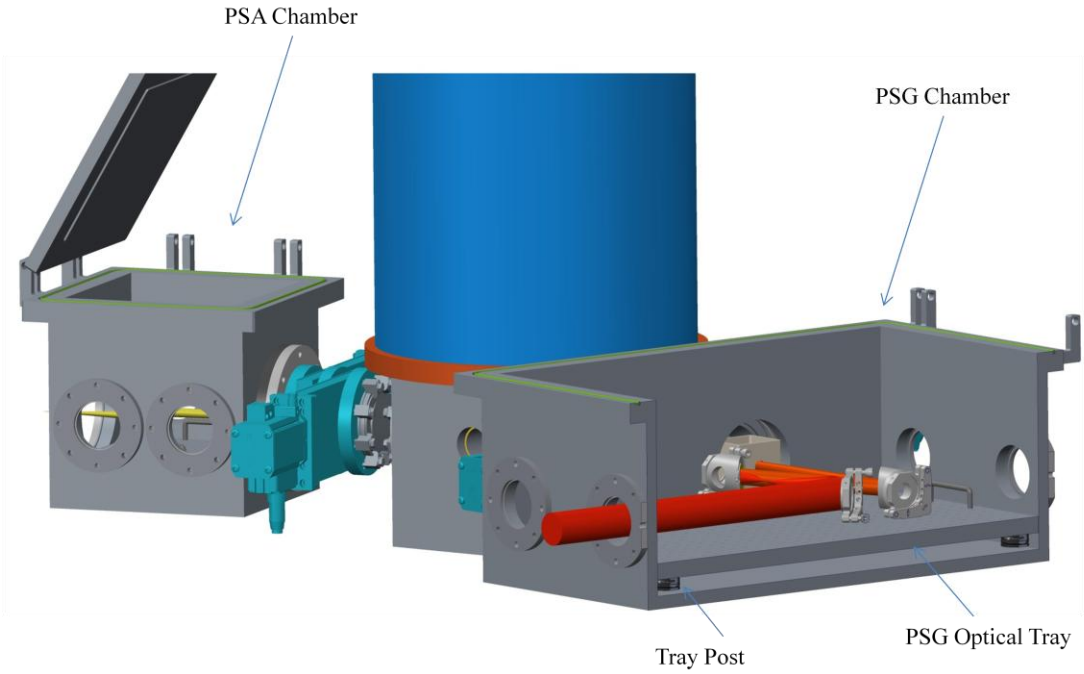

Figure 4.9 Shows the Optical tray holder mechanism. The tray has four standoffs, located at each corner of the optical tray. The standoffs provide maximum repeatable X-Y-Z positional location for best optical alignment.

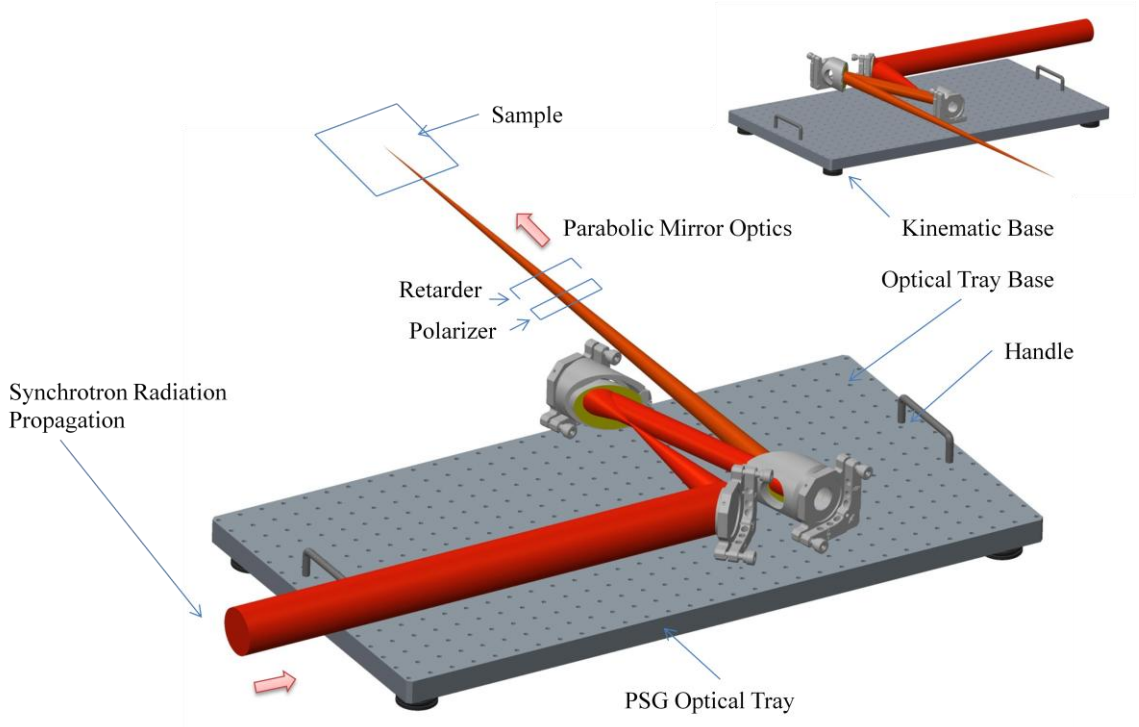

Figure 4.10 Optical tray system – the tray is designed to be removable for easy use and efficiency.

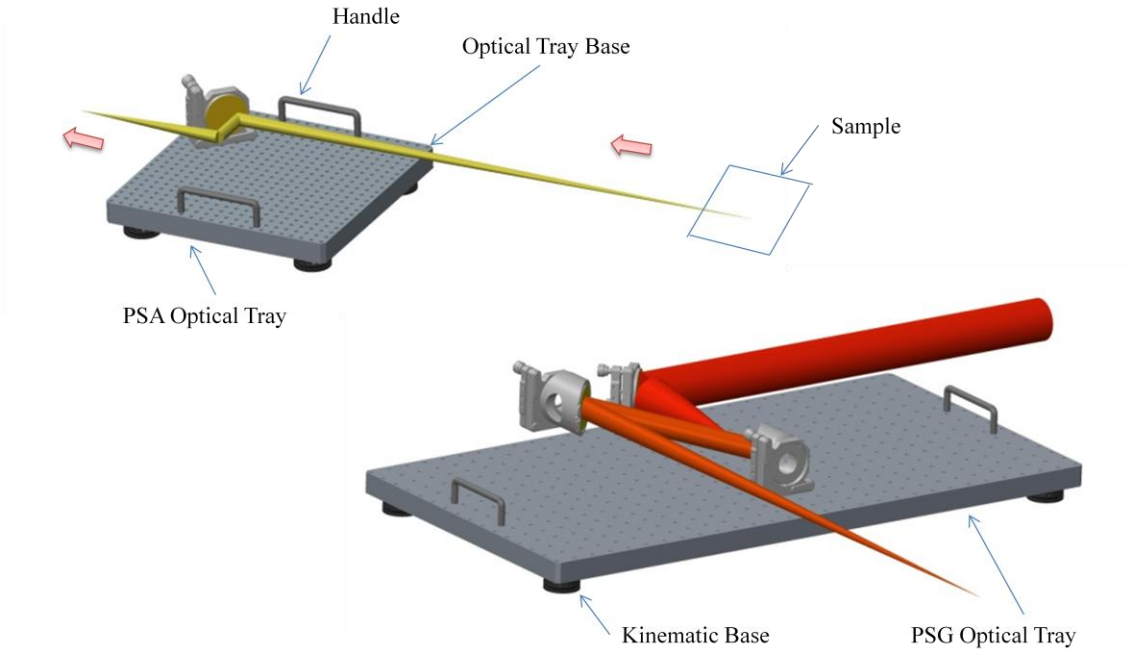

Figure 4.11 Optical tray system – the standoffs can be seen in the view. Here both PSG optical tray (one the right side) and PSA on the left side is shown. Light propagation is a cartoon. The real ZEEMAX simulation is shown in Fig. 4.3.

4.3 Magnetic Field Solution

The main idea of this Project is to build an optical system where a sample will be placed in a magnetic field. The main questions that we have to justify are related to the magnetic field strength and its orientation with respect to the sample surface. Here we propose a compromise between two possible approaches: (i) to choose the strongest available magnet or (ii) to select a magnet model with moderate field but flexible in terms of the field orientation and economical in terms of operations. Let's justify the second approach. The optical magnet is proposed to become a central piece at the MET beamline of NSLS-II. In contrast to a single Investigator Lab at a regular University, we expect a nearly non-

stop operation regime with different Users arriving to NSLS-II from USA and abroad. The cost of operation for a LHe-cooled magnet may become prohibitively expensive for the most of potential Users: ~20 lit of LHe/day at the current cost of ~ $14/litter, just to keep the system cold plus a 50% increase for strong field operations. Taking into account possible shortages with LHe supply and the absence of the centralized LHe recovery system at NSLS-II beamlines, we restrict our choice of the optical magnets to LHe-free systems only.

The second requirement is to have a horizontal field in a "split-coil" magnet configuration with four optical ports located at 90 deg with respect to each other. This system has the main advantage: one can reconfigure optics between two main experimental configurations: Faraday and Voigt. This process will take about 4 days because it requires a complete warm up of the magnet and a break of the magnet vacuum with a consequent pumping and cooling of the magnet. In the Faraday configuration the magnetic field is directed normal to the sample surface or along *Z*. In the Voigt geometry the magnetic field is directed parallel to the sample surface, or along *X*-direction. Note here that in a few existing ellipsometers with a magnetic field option, the measurement geometry is cumbersome and tricky for data analysis and interpretation: the light is reflected in a 90 deg configuration and the field is applied at 45 deg with respect to the sample plane. [34,35,36]

The commercially available "LHe-free" systems from the major equipment suppliers, such as OXFORD, JANIS, CRYOGENIC, *etc*, have two standard

configurations for the maximum field of either 7 T or 10 T. The common feature of the stronger field systems is a great increase of their *f*# for the optical ports (equivalent to a decrease of the NA). For example, the 10 T system from OXFORD has an *f*#=5.9 vs. *f*#=3 for 7 T system. In simple words, larger *f*# corresponds to a longer solenoid with the same or even smaller inner tube diameter. For optical experiments at an oblique incidence, that means a "slow" focusing on the sample, larger AOIs, and the corresponding increase of the spot size on the sample surface. The latter may not be acceptable for small multiferroic or superconducting single crystals, which are usually available only with a few mm^2 surface area. At the same time, large *f*# means a long-wavelength cutoff. Our estimates show that a 10 T solenoid would cut most of the light intensity below ~ 40 cm^{-1}, while a 7 T magnet with *f*#=3 would allow us to measure confidently down to ~ 20 cm^{-1}. The standard commercial products should also have an advantage or reliability and quicker delivery time compared to a custom-made magnet designed for high fields.

The National Research Council Report [1] listed about 20 high magnetic field beamlines at the National and International Synchrotron and Neutron facilities. It is interesting to note that the "average" highest available magnetic field at all those Facilities is about 10 T. Thus, our choice of the magnet falls close to the average. We propose to select a LHe-free split-coil 9 T optical magnet with a relatively small *f*#=3.

4.4 Vacuum Solution

One of the main obstacles in low-temperature ellipsometry is windows that separate the sample volume from the polarizers/compensators. Especially bad are cold windows whose optical properties may change with temperature and even with the history of cooling. It is important to note that the optical properties of windows may also strongly change with the magnetic field due to Faraday rotation, thus making accurate ellipsometry measurements practically impossible. A distinct feature of this project is a design of an ellipsometer without cold-windows. The sample volume and the polarizer/compensator volumes will be separated by a pair of 6 micron-thick mylar windows during the measurements. As one can see in Figs. 4.1 and 4.2, the sample is introduced close to the center of the magnet using a flexible bellow and a long-travel distance Z-stage. Two optical chambers, PSG and PSA, are connected to the magnet using flexible HV bellows. The flexible bellows are required for adjustment of the AOIs, PSA alignment, and for relive of the strains that could be built otherwise at the PSG-magnet-PSA joints. For the purpose of the optics exchange and alignment, such as a switch between RAE, RCE, and MM-SE experiments, the optics chambers will be separated from the magnet volume with two pairs of gate valves on both optical ports. The gate valves close to the magnet shroud will be equipped with "hard" optical windows needed for alignment purpose. These windows will be thick enough to sustain 1 atm differential pressure. For safety of operation, these "hard window" gate valves will be equipped with quick and automatic pressure-enabled shut-down system. The second pair of gate valves will have 6 micron mylar windows, which cannot sustain more than 0.05 atm, but are perfect for ellipsometry measurement and for separation of the vacuum

volumes inside the magnet (~ 10^{-7} Tor) and in PSA and PSG chambers (~10^{-3} Tor). For alignment and optics exchange in PSA/PSG, the hard windows are in place, mylar windows are out. For the actual ellipsometry measurements, the mylar windows are in, then the hard windows are out (see Figure 4.12 and 4.13). Here we note that the existing Ellipsometer at U4IR beamline of NSLS had a pair of 6-micron thick mylar windows positioned between the PSG-sample-PSA volumes. This ellipsometer was operational for ~ 1 year without a single accident that resulted in a mylar window damage. Both PSA and PSG chambers are designed for HV operations that will improve safety of operations. The motorized stages for polarizers and mirrors are HV-compatible. The motors will be shifted away from the strong straight field area and will be coupled to the gears with long shafts (or timing belts).

The entrance to the PSA chamber and the exit port of the PSA chamber will be equipped with hard IR windows. Note that this external pair of windows does not influence the quality of the MM-SE measurements because the PSG section will have a *P0* polarizer, while PSA analyzer *A* is usually stationary in both, RCE and MM-SE experiments. The "price" for the luxury of using window-free design is a higher cost of the HV-graded vacuum chambers and an extra turbo pump for the volume between two gate valves.

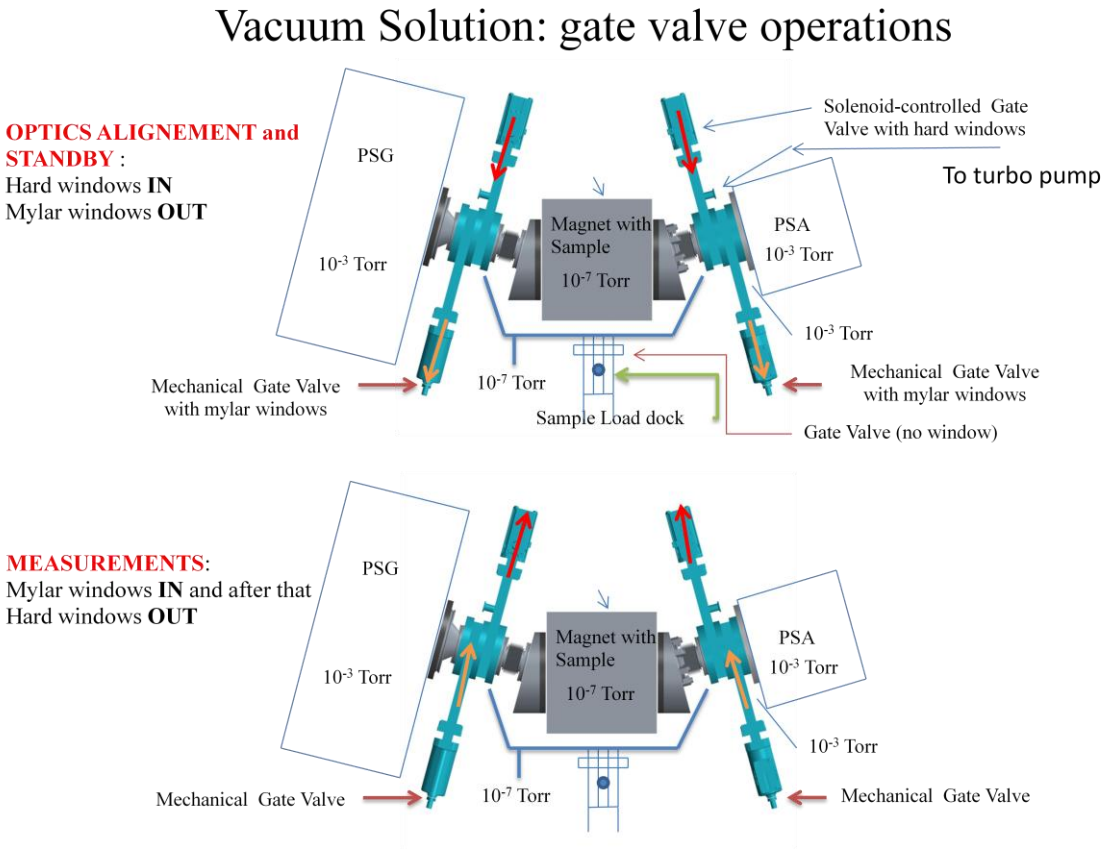

	Normal Operation					
	PSG Valves	Loading Dock Valve	PSA Valves			
Mechanical	Solenoid	Solenoid	Solenoid	Mechanical	Operation	Vacuum
↑	↓	↓	↓	↑	Initial Condition	PSG + PSA 10^{-3} Torr
		Load Sample			Load sample	draw vacuum 10^{-7} Torr
↑	↓	↑	↓	↑	Load sample	
↑	↓	←	↓	↑	Load sample	
↓	↑	←	↑	↓	Set & Test	

Figure 4.12 Positioning of the gate valves when instrument is in standby position and in the measurement state.

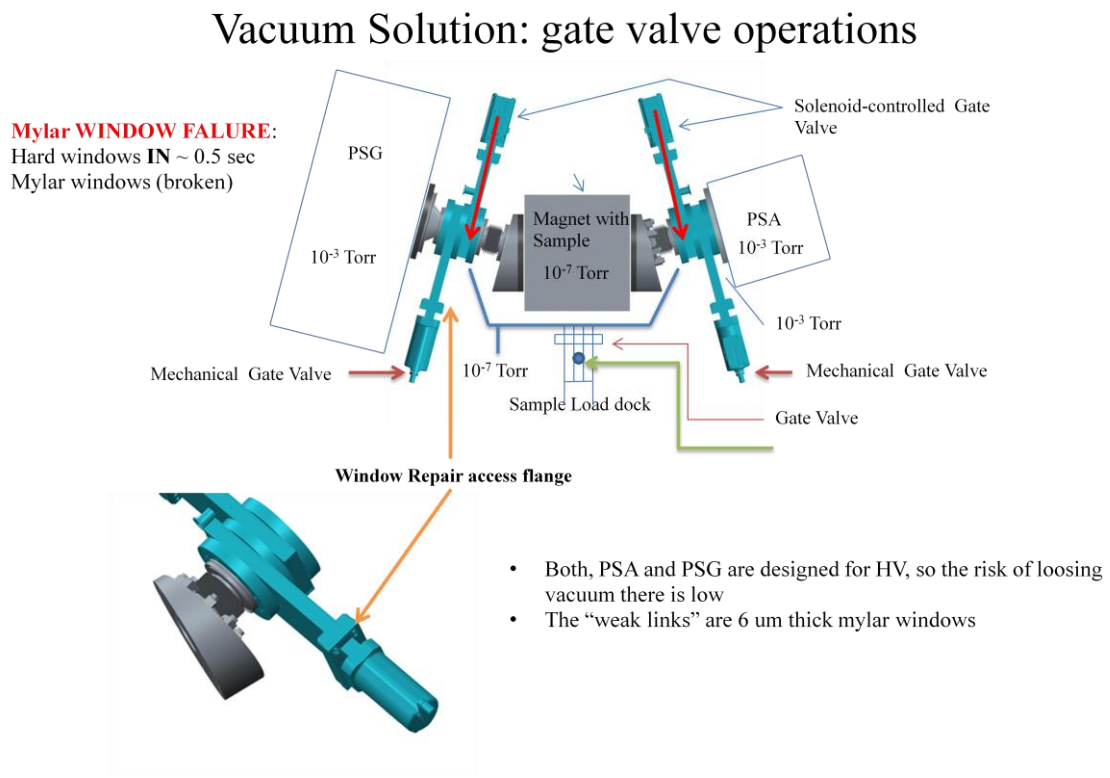

	Mylar Window Failure					
	PSG Valves	Loading Dock Valve	PSA Valves			
Mechanical	Solenoid	Solenoid	Solenoid	Mechanical	Operation	Vacuum
↓	↓	←	↓	↓	Initial Condition	PSG + PSA 10^{-3} Torr
↑	↓	←	↓	↑	Remove Mylar Window	PSG + PSA at Atmosphere
↑	↓	←	↓	↑	Replace Mylar Window	PSG + PSA at Atmosphere
↑	↓	←	↓	↑	Draw Vacuum	PSG + PSA 10^{-3} Torr
↓	↓	←	↓	↓	Draw Vacuum	Gate Valves 10^{-3} Torr
↓	↑	←	↑	↓	Set & Test	

Figure 4.13 Positioning of the gate valves when Mylar window fails and thereafter replacement of the window – Getting to normal operation.

4.5 Solutions for the Sample Cooling to Low Temperatures

Optical spectroscopy of correlated materials requires low temperatures. On one hand, an ideal for us cryostat system should allow for sample cooling down to 1.6 K. On the other hand, to satisfy this requirement we would have to put our samples in LHe vapor or inside superfluid liquid. Ultimately, our cryostat would require a set of cold windows thus making the accurate ellipsometry measurements very difficult. Here we propose a solution that has a sample on a cold finger in vacuum at temperatures down to T =4 K and no windows geometry for ellipsometry. At the end of this Section we will also describe an additional option to have a separate sample VTI section, which will allow for simple polarimetry studies in conventional transmission/reflection geometries for samples in pumped LHe at temperatures down to T=1.6 K.

As shown in Figure 4.2, the sample is positioned in the HV volume sharing vacuum with the solenoid. This idea has been first implemented by Ken Burch , now at Boston College [120], and then also implemented in Basov's (UCSD) and Kuzmenko's (U.Geneva) Labs. The lowest temperature, which could be achieved at the sample position is about 4 K. The sample cooling is provided by continuous flow of LHe in a Supertran-type of a cryostat inserted inside the magnet through one of the optical ports. This configuration has become a standard options for all major suppliers of optical magnets, such as OXFORD, JANIS, and CRYOGENIC. The sample exchange is enabled with a long-range traveler. The sample loading position is separated from the magnet volume with a gate valve. Thus, the magnet can be kept cold while the samples are exchanged trough the loading dock window. The Supertran -type of cryostats are

economical and require between 5 and 10 liters of LHe per experimental day depending on the temperature range of the experiment. For the high temperatures one can easily substitute LHe with LN2 thus saving experimental supplies. The low LHe consumption during the experiments should allow He gas recovery using, for example, commercially available *Cryomech* equipment.

A certain class of samples, especially those with ultra-low spin-ordering temperatures, such as multiferroics with R^{3+} ions, may require cooling below 4 K. For this case we propose to include a separate option for transmission/reflection experiments with a sample inside a VTI volume loaded from the top port of the magnet. The side-load system will be, of course, retracted and separated from the magnet volume with a gate valve. Installation of the VTI will require a complete warming up of the magnet, same as for the switch between the Faraday and Voigt configurations. The proposed VTI inset will have 2 diamond windows at 90 deg for experiments in a broad spectral range. Both, transmission and reflection configurations will be possible. Even more, with two bolometers, transmission and reflection spectra could be measured simultaneously using two channels of the BRUKER interferometer. The sample volume will be filled up with LHe from the top using a transfer line (~ 5 lit/experimental day). After that the VTI volume will be pumped and 1.6K temperature can be reached.

4.6 Optics Solutions / Light Propagation

The infrared synchrotron radiation after the diamond window is collimated and transported to a spectrometer, for example the existing Bruker IFS 66v FT-IR, with a full

complement of beamsplitters to span the spectral range from far-IR to visible light. The best available spectral resolution of the installed spectrometer is 0.3 cm^{-1}. After passing the interferometer, the IR radiation is directed to the ellipsometer. The optical path inside the Ellipsometer is shown in Figure 4.3. Qualitatively, the optical configuration is similar to that for the existing MM-SE setup at U4IR-NSLS. The main quantitative difference is a reduction of the *f*# from original *f*#=20 down to *f*#=15. The latter will provide a smaller beamsize on the sample, while the quality of polarization control will be slightly compromised. The light beam with a cross-section of 50×50 mm^2 is first folded and compressed inside the PSG chamber for alignment purpose using a pair of the off-axis parabolic mirrors, M1 and M2. The initial state of polarization, which is linearly polarized in the vertical direction, is conditioned with an additional P0 linear polarizer (not shown in Figure 4.3). After that the synchrotron radiation is focused using M3 off-axis parabolic mirror. A pair of polarization-control components, a polarizer *P* and retarder (=compensator) *C1* are positioned in the focused beam where the cross-section of the beam is reduced below 20×20 mm^2. The focusing parabola on a motorized kinematic mount provides a beam alignment capability. The sample reflects the light to the PSA chamber at a glancing angle of incidence (AOI=75 deg in Figure 4.3). The optical components in PSA are just a mirror image of that in the PSG chamber: a pair of *C2* retarder and an analyzer *A*. An elliptical mirror focuses the light on a bolometer. This optical setup is robust against the changes of AOI in the range between 70 and 85 deg and also allows for a nearly alignment-free conversion to transmission/reflection configuration.

4.7 Ellipsometry Solutions

Our design accommodates all standard requirements for ellipsometry measurements, such as a full control of the light polarization in both, PSA and PSG sections, variable AOI, and motorized alignment options for both the sample position inside the magnet and focusing mirrors. Thus, here we propose a full Mueller Matrix ellipsometer with a sample in magnetic field. Since from the polarization-control point of view our new ellipsometer will be similar to the existing U4IR ellipsometer, we will describe this part very briefly. More details could be found in our recent review Ref. [8] Full Mueller matrix ellipsometry requires a complete polarization coverage of the Poincare sphere. This can only be achieved by using rotating optical retarders. The classical arrangement of the light propagation between polarizers and retarders is implemented in the most of professional ellipsometers as follows: P → C1 → Sample → C2 → A → Detector. For the projected spectral range between 20 and 4000 cm^{-1}, we will use three sets of the linear polarizers *P* with a 25 mm diameter: (i) free-standing wire grids (20 – 200 cm^{-1}), (b) wire grids on polyethylene substrates (30 – 700 cm^{-1}), and (iii) wire grids on KRS5 substrates (400 – 4000 cm^{-1}). Optical retarders for far-IR spectral range have been developed and manufactured by our Group during the previous NSF-MRI Project. As described in Equipment and Other Recourses Section, we already have several sets of the rotatable retarders: (i) single semi-insulating Si prism, (ii) double-Fresnel Si prisms, (iii) double-Fresnel KRS prisms, and (iv) single ZnSe prism. Their corresponding spectral ranges are 20 – 500 cm^{-1}, 400 – 1000 cm^{-1}, and 800 – 4000 cm^{-1}.

CONCLUSIONS

The presented here design of the Mueller matrix spectroscopic ellipsometer with high magnetic field up to 9 Tesla is potentially useful for analysis of electromagnetic materials at the MET beamline of NSLS-II, BNL. The new instrument includes a possibility for a quick switching between Faraday to Voigt configuration for the magnetic field direction and also between the ellipsometry, transmission, and reflection optical configurations. Such reconfiguration of the setup is provided by a combination of the flexible bellows, adapter plates, and 90 deg invariants for the mechanical design of the 4-port optical magnet.

A safe and convenient way to switch between the standby, alignment, and measurement regimes is provided by the double-gate valve solution for mounting of the optical windows, which separate the PSA, PSG, and magnet sections of the setup that operate at pressure of 10^{-3} and 10^{-7} Torr, respectively. In addition, if the ultrathin mylar windows fail due to mechanical damage, the instrument that is equipped with solenoid-enabled gate-valves is designed to switch automatically to the safe standby mode in less than 1 second. The repair time for mylar windows would be less than 1 hour. Thus the instrument maintenance and repair time is minimized and precious operational beamtime at MET, NSLS-II can be preserved for important measurements.

This instrument is designed for measurements of the samples at very low temperature of 4.2 K. The sample exchange is enabled by a side loading dock that is separated with manually-operated gate valve so that samples could be quickly loaded to the center of the magnet in less than 1 hour. Sample alignment is available along the motor-controlled *z*-axis, as well as in three orthogonal angular directions: *Omega*, *Phi*,

and *Chi* axes. The design allows for a wide range of sample alignment motion ±4° for *Omega* and *Chi* axes and for 360° continuous motion in *Phi* direction. The mechanical compensation for the sample displacement during alignment is provided by three flexible bellows used in the design.

Parabolic mirrors are used in the optical design to compress the incoming synchrotron radiation beam to the desired ½" size that enables the use of the standard Mueller Matrix ellipsometry optics, such as the IR polarizers and broadband retarders. The parabolic mirrors provide zero spherical aberration. The optics is optimized for the spectral range of 20 cm^{-1} to 4000 cm^{-1}. For quick changes in the optical layout all optical components, such as mirrors, polarizers, retarders and apertures are designed to be mounted on optical trays with kinematic bases. This approach allows us to minimize optics misalignment during pumping the whole instrument down to the base pressure of 10^{-3} Torr.

The complete design of our ellipsometer is documented in a set of 2D and 3D professional drawings that may safe a significant amount of funding for the Project compared to design outscoring to, for example, the optical magnet manufacturer.

APPENDIX

DRAWINGS

Figure A.1 to A.11 show the 2D drawing of machine components.

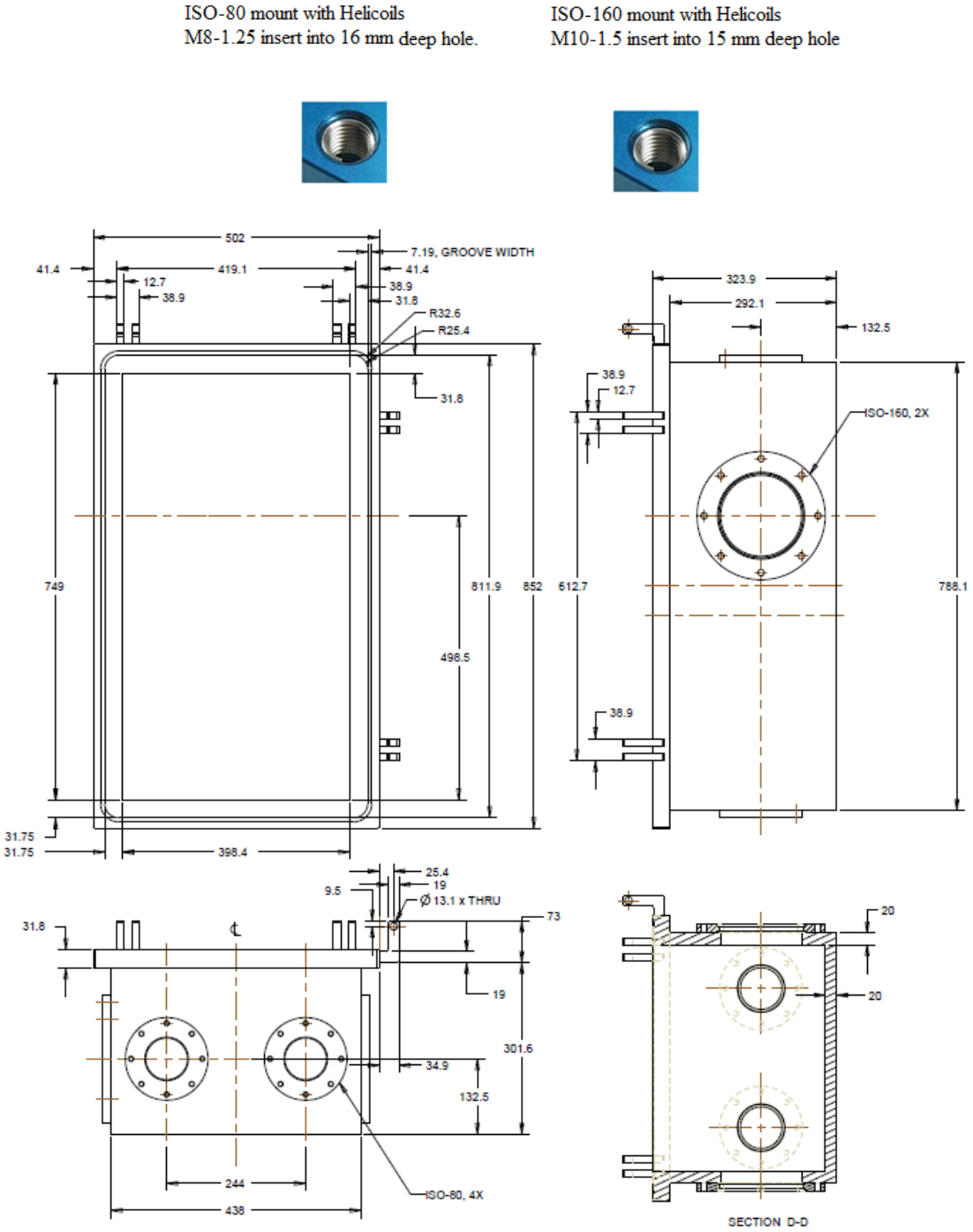

Figure A.1a 2D drawing for the Polarization State Generation (PSG) chamber.

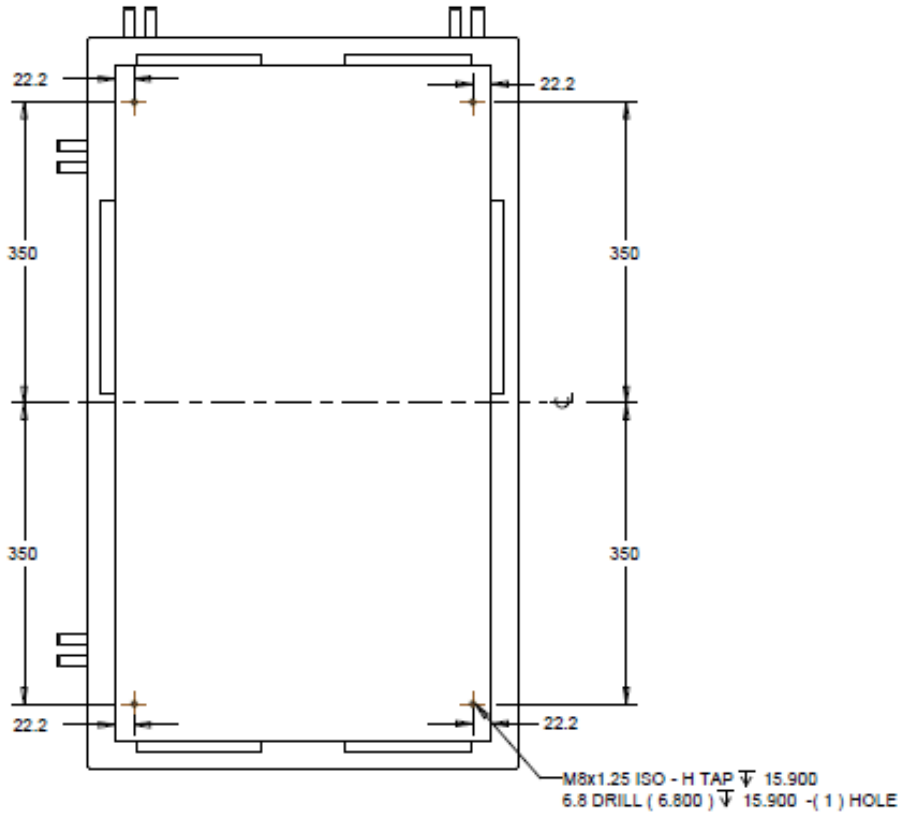

Figure A.1b 2D drawing for the Polarization State Generation (PSG) chamber (Bottom view).

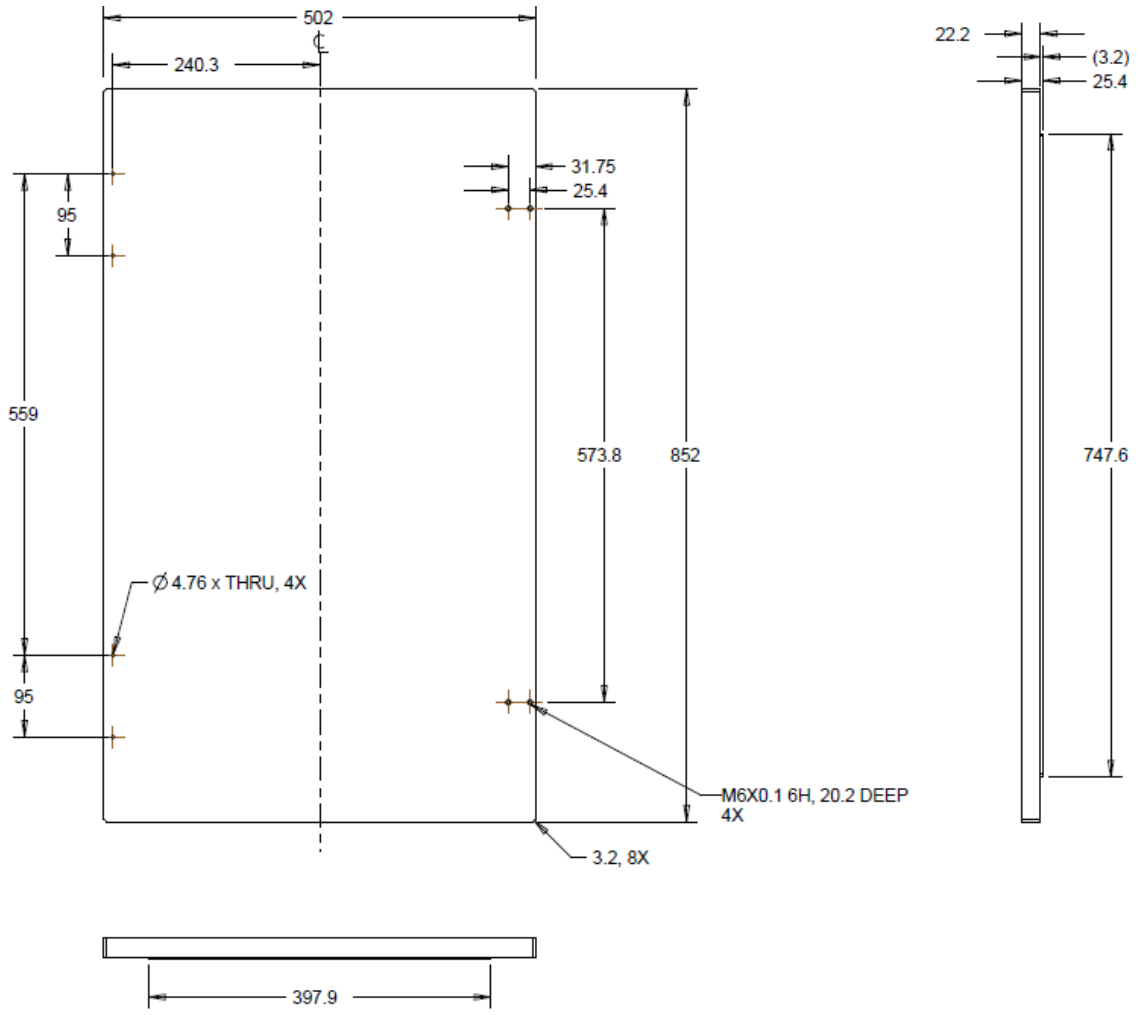

Figure A.2 2D drawing for the Polarization State Generation (PSG) chamber lid. Handle McMaster Carr P/N 1568A490 is mounted into hole dia. 4.76 (4X) with M4-18 screws (McMaster P/N 92000A227).

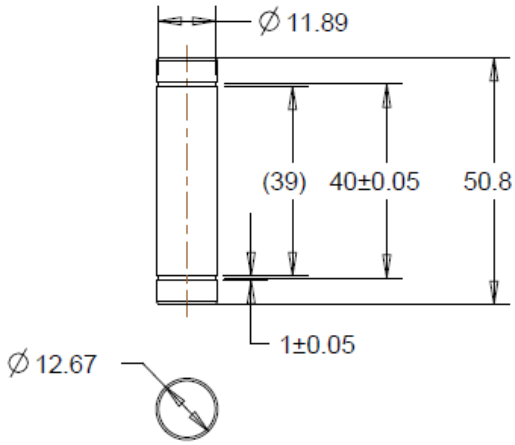

Figure A.3 2D drawing for the Hinge Pin for the PSG and PSA chamber. The Pin is used with Spiral Ring (McMaster P/N 91650A420.

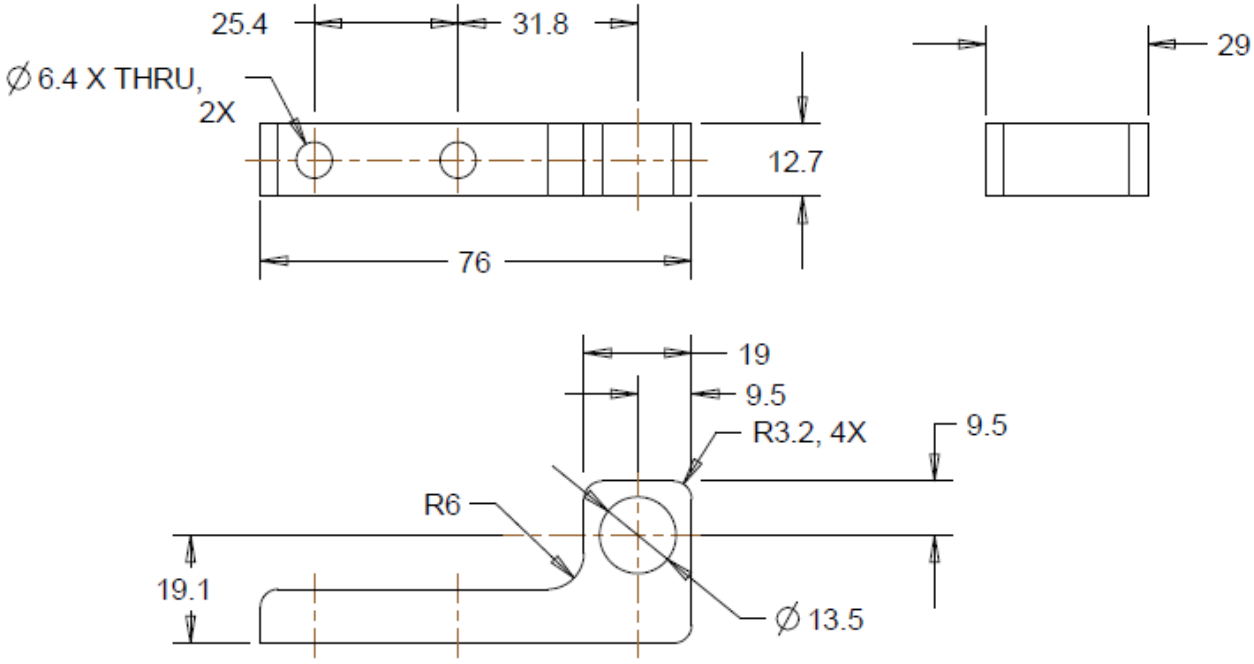

Figure A.4 2D drawing for the Hinge Lid for the PSG and PSA chamber. The part is assembled with Pin (drawing 4.3) and Spiral Ring (McMaster P/N 91650A420.

ISO-80 mount with Helicoils
M8-1.25 insert into 16 mm deep hole.

ISO-160 mount with Helicoils
M10-1.5 insert into 15 mm deep hole

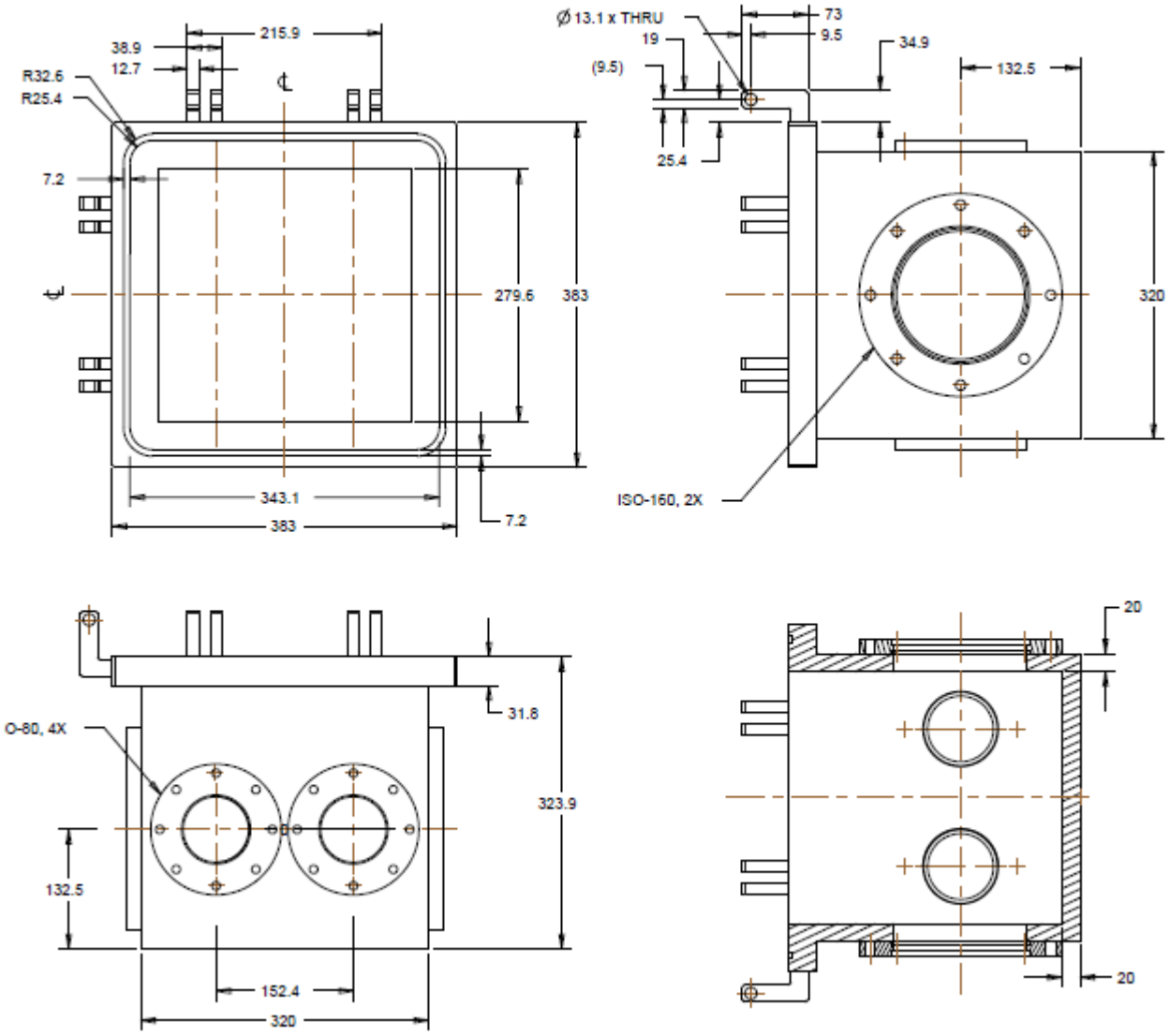

Figure A.5 2D drawing for the Polarization State Analyzer (PSA) chamber.

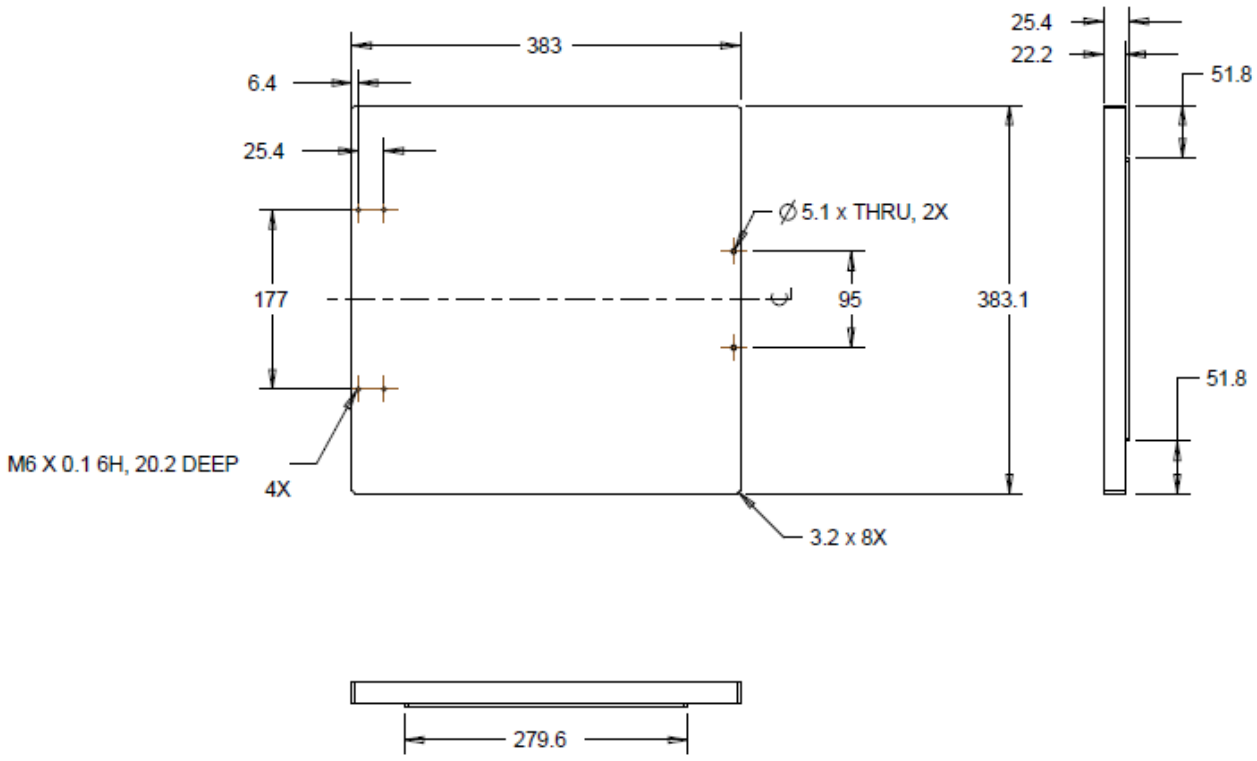

Figure A.6 2D drawing for the Polarization State Analyzer (PSA) chamber lid. Handle McMaster Carr P/N 1568A490 is mounted into hole dia. 4.76 (4X) with M4-18 screws (McMaster P/N 92000A227).

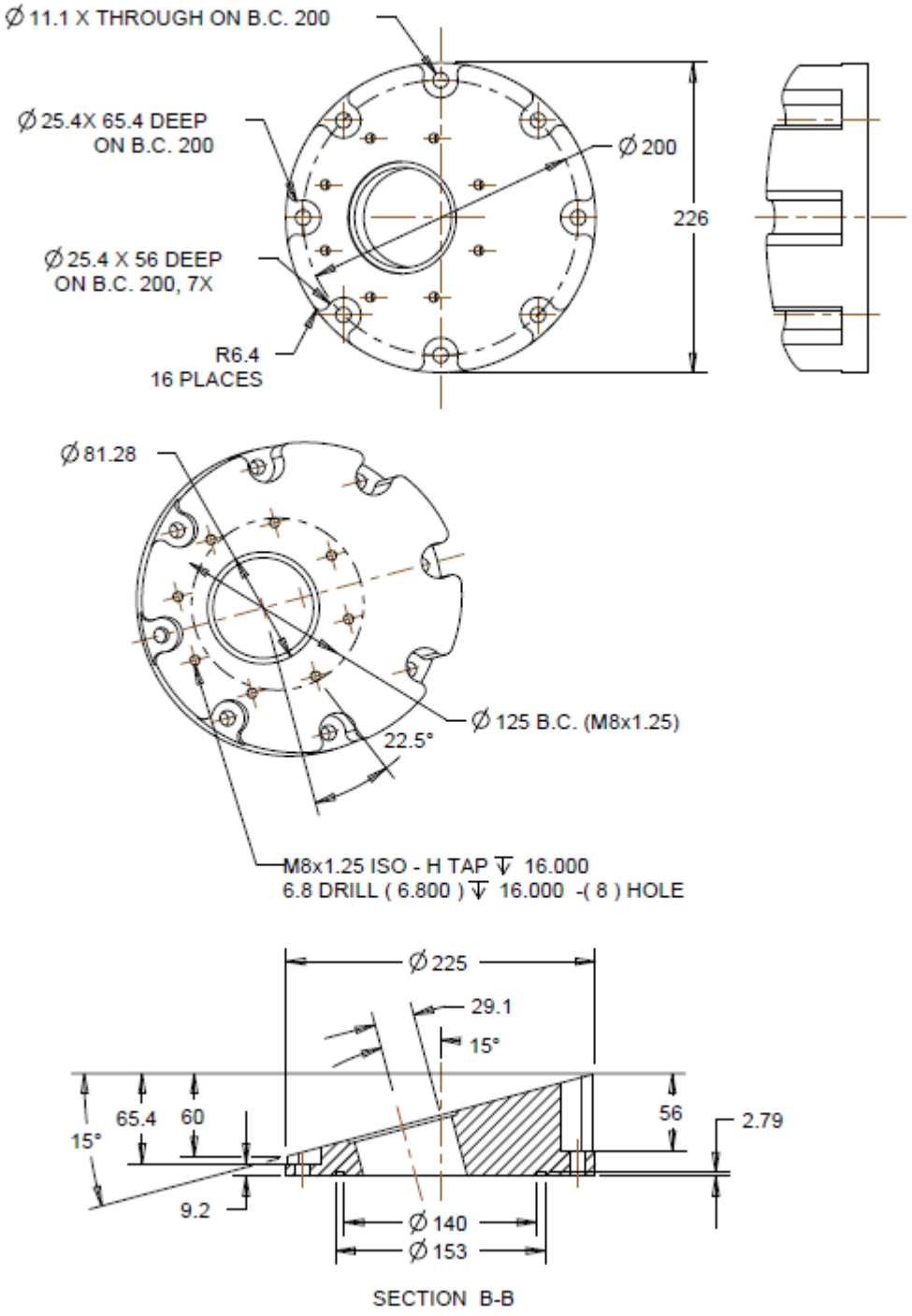

Figure A.7 2D drawing of the 15° Adopter.

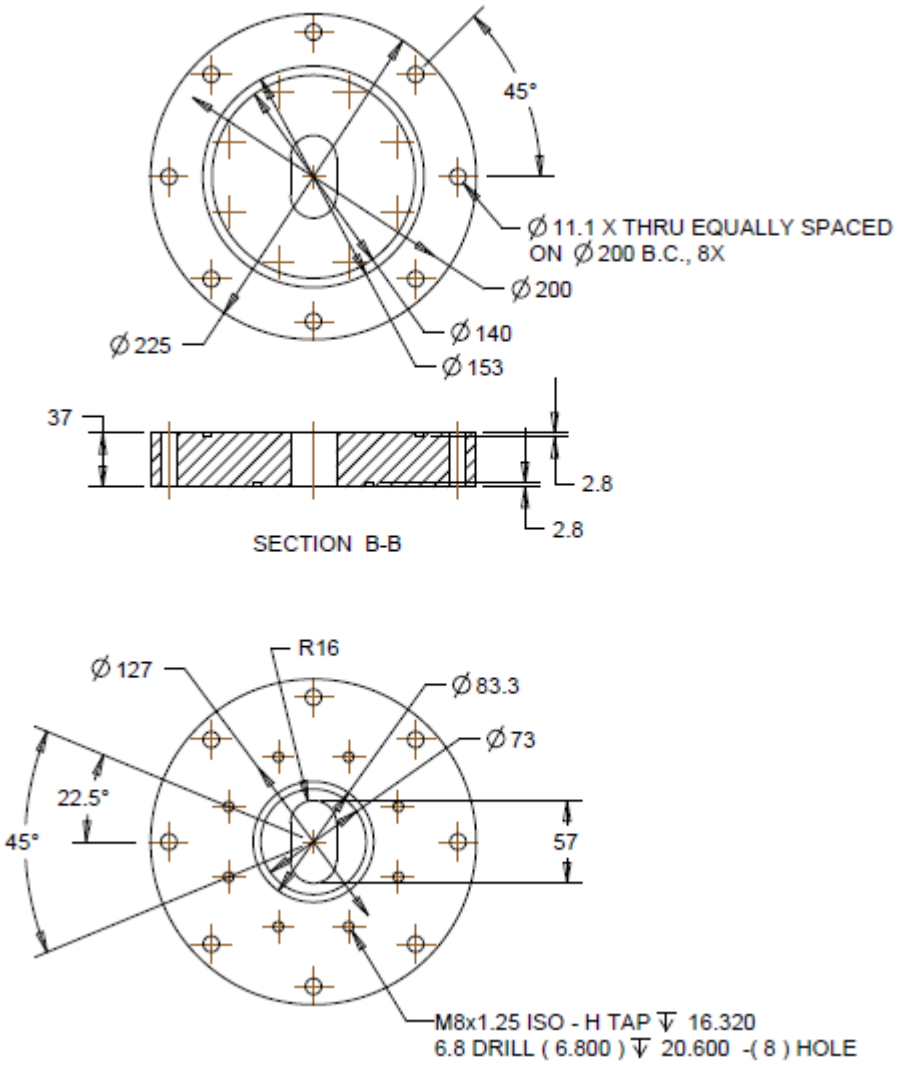

Figure A.8 2D drawing for the 90° Adopter.

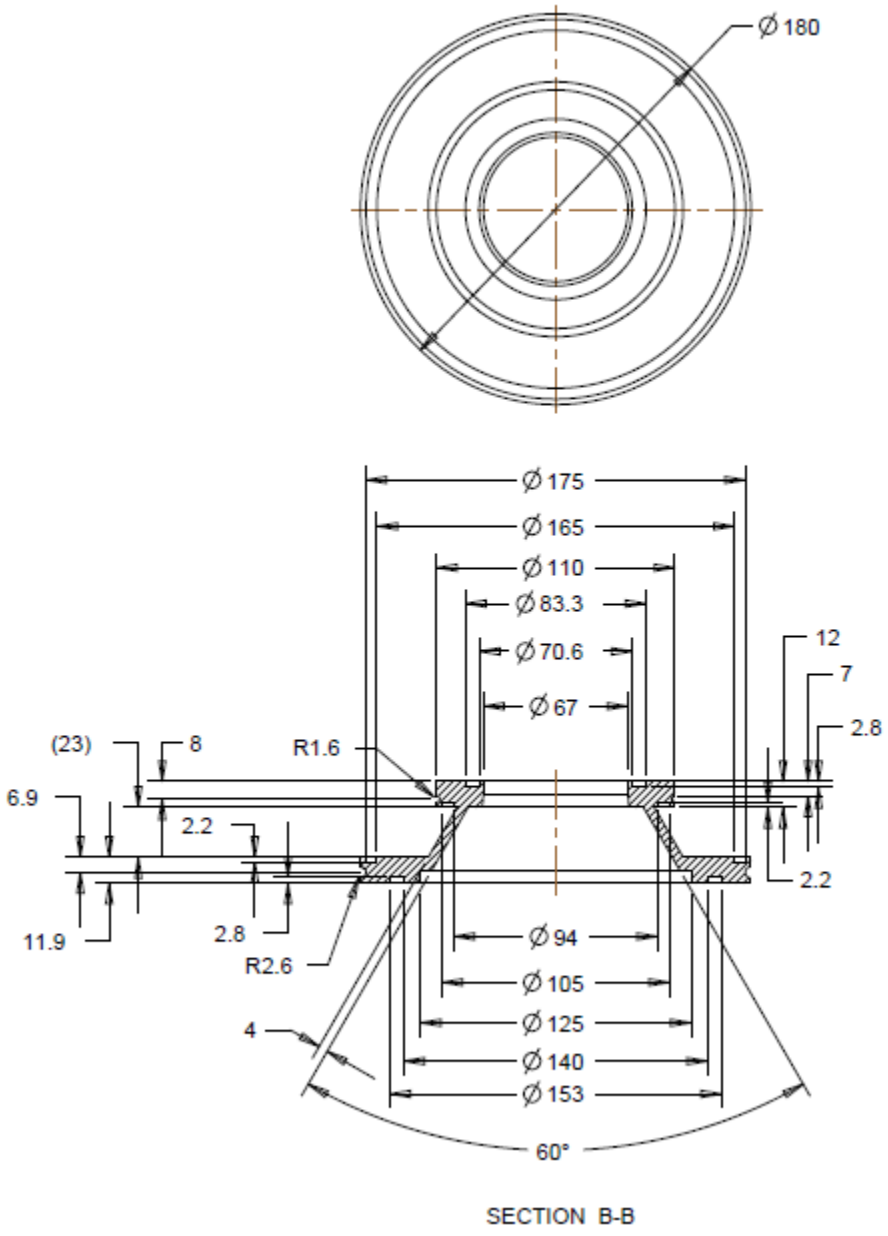

Figure A.9 2D drawing for the Conical Adopter.

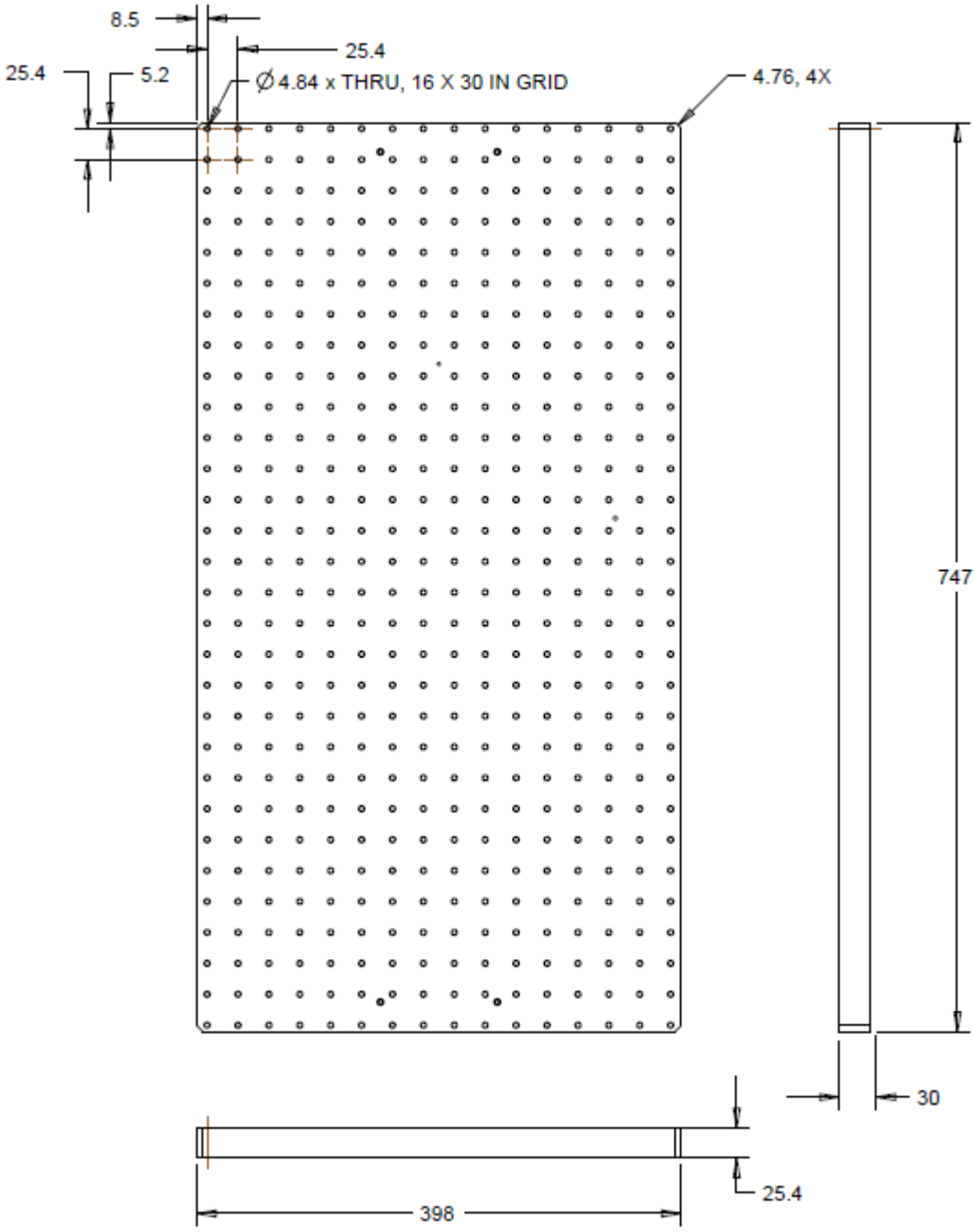

Figure A.10 2D drawing for the PSG Optical base plate.

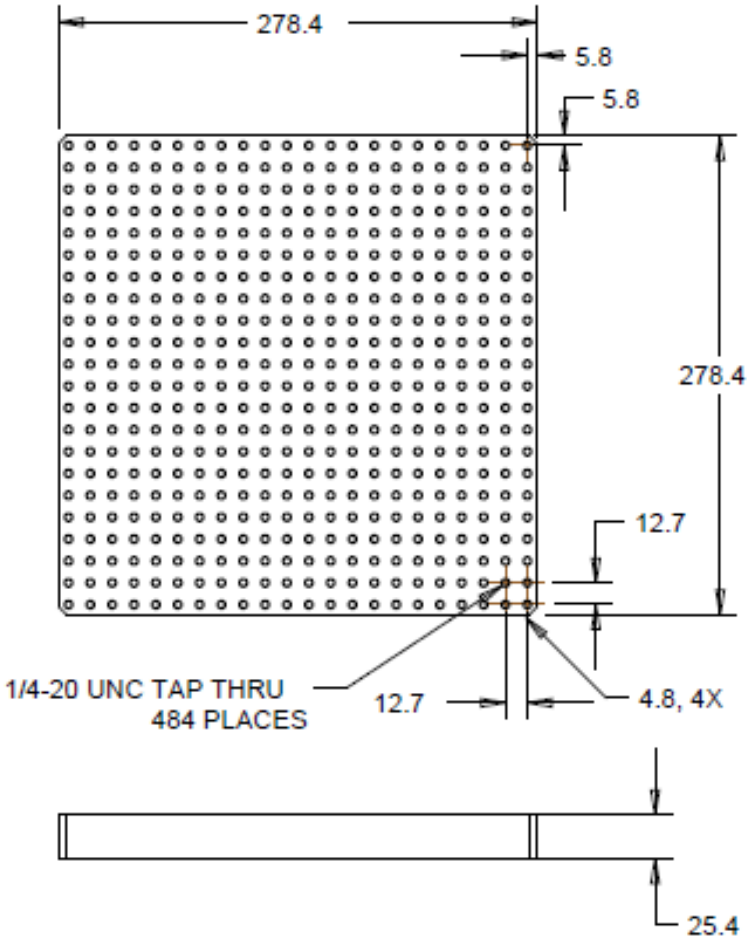

Figure A.11 2D drawing for the PSA Optical base plate.

REFERENCES

1. "High Magnetic Field Science and Its Application in the United States: Current Status0 and Future Directions", the National Academies Press (2013) ISBN: 978-0-309 -28634-3.

2. C. J. Hirschmugl and G. P. Williams, *Infrared Synchrotron Radiation: Programs at the NSLS,* Synchrotron Radiation News **8**, 10 (1995).

3. P. S. Hauge, J. Opt. Soc. Am. **68**, 1519 (1978).

4. P. D. Rogers, T. D. Kang, T. Zhou, M. Kotelyanskii, and A. A. Sirenko, "*Mueller matrices for anisotropic metamaterials generated using 4×4 matrix formalism*", Thin Solid Films , **519**, 2668 (2011).

5. T. D. Kang, E. Standard, G. L. Carr, T. Zhou, M. Kotelyanskii, and A. A. Sirenko, "*Rotatable broadband retarders for far-infrared spectroscopic ellipsometry*", Thin Solid Films, **519**, 2698 (2011).

6. Xiaoxiang Xi, R. J. Smith, T. N. Stanislavchuk, A. A. Sirenko, S. N. Gilbert, J. J. Tu, and G. L. Carr, "*A broadband silicon quarter-wave retarder for far-infrared spectroscopic circular dichroism*", Infrared Physics & Technology **67**, 436–440 (2014).

7. P. D. Rogers, Y. J. Choi, E. C. Standard, T. D. Kang, K. H. Ahn, A. Dubroka, P. Marsik, Ch. Wang, C. Bernhard, S. Park, S.-W. Cheong, M. Kotelyanskii, and A. A. Sirenko, "*Adjusted oscillator strength matching for hybrid magnetic and electric excitations in $Dy_3Fe_5O_{12}$ garnet*", Phys. Rev. B **83**, 174407 (2011).

8. T. N. Stanislavchuk, A. A. Sirenko, A. P. Litvinchuk, X. Luo, and S.-W. Cheong, "*Electronic band structure and optical phonons of $BaSnO_3$ and $Ba_{0.97}La_{0.03}SnO_3$ single crystals: Theory and experiment*", J. Appl. Phys. **112**, 044108 (2012).

9. T. D. Kang, E. C. Standard, P. D. Rogers, K. H. Ahn, and A. A. Sirenko, A. Dubroka, C. Bernhard, S. Park, Y. J. Choi and S.-W. Cheong, "*Far-infrared spectra of the magnetic exchange resonances and optical phonons and their connection to magnetic and dielectric properties of $Dy_3Fe_5O_{12}$ garnet"*, Phys. Rev. B **86**, 144112 (2012).

10. D. W. Jeong, Woo Seok Choi, T. D. Kang, C. H. Sohn, A. David, H. Rotella, A. A. Sirenko, Cheol Hyeok Lee, Jae H. Kim, U. Lüders, W. Prellier, Y.-J. Kim, Yun Sang Lee, and T. W. Noh, "Optical spectroscopy of the carrier dynamics in LaVO3/SrVO3 superlattices", Phys. Rev. B **84**, 115132 (2011).

11. R. Basistyy, T. N. Stanislavchuk, A. A. Sirenko, A. P. Litvinchuk, M. Kotelyanskii, G.L. Carr, N. Lee, X. Wang, and S.-W. Cheong, "*Infrared-active optical phonons and magnetic excitations in the hexagonal manganites $RMnO_3$ (R = Ho, Er, Tm, Yb, and Lu)*", Phys. Rev. B **90**, 024307 (2014).

12. K. N. Boldyrev, T. N. Stanislavchuk, A. A. Sirenko, L. N. Bezmaternykh, and M. N. Popova, "*Coupling between phonon and crystal-field excitations in multiferroic PrFe3(BO3)4*", Phys. Rev. B**90**, 121101(R) (2014).

13. D. Pröpper, A. N. Yaresko, T. I. Larkin, T. N. Stanislavchuk, A. A. Sirenko, T. Takayama, A. Matsumoto, H. Takagi, B. Keimer, A. V. Boris, "*Fano Resonances in the Infrared Spectra of Phonons in Hyperkagome $Na_3Ir_3O_8$*", Phys. Rev. Lett. **112**, 087401 (2014).

14. O. Caha, A. Dubroka, J. Humlícek, V. Holý, H. Steiner, M. Ul-Hassan, J. Sánchez Barriga , O. Rader , T. N. Stanislavchuk, A. A. Sirenko, G. Bauer, and G. Springholz, "*Growth, Structure, and Electronic Properties of Epitaxial Bismuth Telluride Topological Insulator Films on BaF_2 (111) Substrates*", Cryst. Growth Des., **13** (8), 3365–3373 (2013).

15. P. D. Rogers, M. Kotelyanskii, and A. A. Sirenko, "*Modeling of electromagnetic wave propagation and spectra of optical excitations in complex media using 4x4 matrix formalism*", arXiv:1105.4934 [physics.optics] , (2011),

16. J. Kircher, R. Henn, M. Cardona, P. L. Richards, and G. P. Williams, ''*Far-infrared ellipsometry using synchrotron radiation*,'' J. Opt. Soc. Am. B **14**, 705–712 (1997).

17. R. Henn, C. Bernhard, A. Wittlin, M. Cardona, and S. Uchida, ''*Far infrared ellipsometry using synchrotron radiation: the out-of-plane response of La22xSrxCuO4* ,'' Thin Solid Films **313-314**, 643–648 (1998).

18. C. Bernhard , R. Henn, A. Wittlin, M. Kläser, G. Müller-Vogt, C.T. Lin, and M. Cardona. *Electronic c-axis Response of Y1-xCaxBa2Cu3O7-δ Crystals Studied by Far-Infrared Ellipsometry*, Phys. Rev. Lett. **80**, 1762 (1998).

19. A. A. Sirenko, C. Bernhard, A. Golnik, Anna M. Clark, Jianhua Hao, Weidong Si, and X. X. Xi, *"Soft-mode hardening in $SrTiO_3$ thin films"*, Nature, **404**, 373 (2000).

20. C. Bernhard, D. Munzar, A. Wittlin, W. König, A. Golnik, C.T. Lin, M. Kläser, Th. Wolf, G. Müller-Vogt, and M. Cardona. *Far-infrared ellipsometric study of the spectral gap in the c-axis conductivity of Y1-xCaxBa2Cu3O7-δ crystals*, Phys. Rev. B **59**, R6631 (1999).

21. C. Bernhard, T. Holden, J. Humlicek, D. Munzar, M. Cardona, and B. Keimer. *In-plane polarized collective modes in detwinned YBa2Cu3O6.95 observed by spectral ellipsometry*, Solid State Commun. **121** , 93 (2002).

22. A.V. Pimenov, A.V. Boris, Li Yu, V. Hinkov, Th. Wolf, B. Keimer, and C. Bernhard, *Ni impurity induced enhancement of the pseudogap in cuprate high Tc superconductors,* Phys. Rev. Lett. **94**, 227003 (2005).

23. C. Bernhard , A.V. Boris, N.N. Kovaleva, G. Khaliullin, A. Pimenov, D.P. Chen, C.T. Lin, and B. Keimer, *Charge ordering and magneto-polarons in* $Na_{0.82}CoO_2$, Phys. Rev. Lett. **93**, 167003 (2004).

24. N. N. Kovaleva, A. V. Boris, C. Bernhard, A. Kulakov, A. Pimenov, A. M. Balbashov, G. Khaliullin, and B. Keimer. *Spin-controlled Mott-Hubbard bands in LaMnO3 probed by optical ellipsometry*, Phys. Rev. Lett. **93**, 147204 (2004).

25. A. V. Boris, N. N. Kovaleva, T. Holden, O. V. Dolgov, C. T. Lin, B. Keimer, and C. Bernhard, *The in-plane spectral weight of charge carriers in* $YBa_2Cu_3O_{6.9}$*: Evidence against kinetic energy driven pairing,* Science **304** , 708 (2004).

26. A. V. Boris, Y. Matiks, E. Benckiser, A. Frano, P. Popovich, V. Hinkov, P. Wochner, M. Castro-Colin, E. Detemple, V. K. Malik, C. Bernhard, T. Prokscha, A. Suter, Z. Salman, E. Morenzoni, G. Cristiani, H.-U. Habermeier, B. Keimer, "*Dimensionality Control of Electronic Phase Transitions in Nickel-Oxide Superlattices*", Science **332**, 937−940 (2011).

27. S.S.A. Seo, W.S. Choi, H.N. Lee, L. Yu, K.W. Kim, C. Bernhard, and T.W. Noh. *Optical study of the free-carrier response of* $LaTiO_3/SrTiO_3$ *superlattices*; Phys. Rev. Lett. **99**, 266801 (2007).

28. A. Dubroka, M. Rössle, K.W. Kim, V. K. Malik, L. Schulz, S. Thiel, C.W. Schneider, J. Mannhart, G. Herranz, O. Copie, M. Bibes, A. Barthélémy and C. Bernhard. *Dynamical Response and Confinement of the Electrons at the* $LaAlO_3/SrTiO_3$ *Interface*; Phys. Rev. Lett. **104**, 156807 (2010).

29. Li Yu, D. Munzar, A.V. Boris, P. Yordanov, J. Chaloupka, Th. Wolf, C. T. Lin, B. Keimer, and C. Bernhard, *Evidence for Two Separate Energy Gaps in Underdoped High-Temperature Cuprate Superconductors from Broadband Infrared Ellipsometry*, Phys. Rev. Lett. **100**, 177004 (2008).

30. A. Charnukha, P. Popovich, Y. Matiks, D. L. Sun, C. T. Lin, A. N. Yaresko, B. Keimer, A. V. Boris. *Superconductivity-induced optical anomaly in an iron arsenide*, Nature Communications **2**, 219 (2011).

31. C. Bernhard, J. Humlıcek , and B. Keimer, *Far-infrared ellipsometry using a synchrotron light source—the dielectric response of the cuprate high Tc superconductors,* Thin Solid Films **455 –456** (2004) 143–149.

32. T. Hofmann, U. Schade, W. Eberhardt, C. M. Herzinger, P. Esquinazi, and M. Schubert, "*Terahertz magneto-optic generalized ellipsometry using synchrotron and blackbody radiation*", Rev. Sci. Inst. **77**, 063902 (2006).

33. A. Röseler, U. Schade, and K. Hoildack, "*Spectral THz ellipsometer for the unambiguous determination of all Stokes parameters*", Infrared and Millimeter Waves and 13th International Conference on Terahertz Electronics, 2005. IRMMW-THz 2005. The Joint 30th International Conference on Volume 1, Issue ,19-23 Sept. 2005 Page(s): 190 - 191 vol. 1.

34. P. Kühne, C. M. Herzinger, M. Schubert, J. A. Woollam, and T. Hofmann, Invited Article: An integrated mid-infrared, far-infrared, and terahertz optical Hall effect instrument, REVIEW OF SCIENTIFIC INSTRUMENTS **85**, 071301 (2014).

35. S. Schöche, T. Hofmann, V. Darakchieva, N. Ben Sedrine, X. Wang, A. Yoshikawa, and M. Schubert, Infrared to vacuum-ultraviolet ellipsometry and optical Hall-effect study of free-charge carrier parameters in Mg-doped InN, J. Appl. Phys. **113**, 013502 (2013).

36. P. Kühne, V. Darakchieva, R. Yakimova, J. D. Tadesco, R.L. Myers-Ward, C.R. Eddy, K. Gaskill, C. M. Herzinger, M. Schubert, and T. Hofmann, Polarization Selection Rules for Inter-Landau-Level Transitions in Epitaxial Graphene Revealed by the Infrared Optical Hall Effect, Physical Review Letters **111**, 077402 (2013).

37. http://optics.unige.ch/wordpress/facilities-2/magnet-room/, (2014)

38. Jason N. Hancock, J. L. M. van Mechelen, Alexey B. Kuzmenko, Dirk van der Marel *et al.*, "Surface state charge dynamics of a high-mobility three dimensional topological insulator", Phys. Rev. Lett. **107**, 136803 (2011).

39. Julien Levallois, Piotr Chudzi´nski, Jason N. Hancock, Alexey B. Kuzmenko, and Dirk van der Marel, "Magnetoplasmon resonances in polycrystalline bismuth as seen via time-domain terahertz spectroscopy", Phys. Rev. B **89**, 155123 (2014).

40. I. Crassee, J. Levallois, D. van der Marel, A. L. Walter, Th. Seyller, and A. B. Kuzmenko, "Multicomponent magneto-optical conductivity of multilayer graphene on SiC", Phys. Rev. B **84**, 035103 (2011).

41. Julien Levallois, Michael Tran, Alexey B. Kuzmenko, "Decrypting the cyclotron effect in graphite using Kerr rotation spectroscopy", Solid State Commun. **152**, 1294- 1300 (2012).

42. http://infrared.ucsd.edu/facilities.html, (2014)

43. W. J. Padilla, Z. Q. Li, K. S. Burch, Y. S. Lee, K. J. Mikolaitis, and D. N. Basov, "Broadband multi-interferometer spectroscopy in high magnetic fields: from THz to visible", Rev. Sci. Instrum. **75**, No 11, 4710 (2004).

44. A. D. LaForge, A. A. Schafgans, S. V. Dordevic, W. J. Padilla, K. S. Burch, Z. Q. Li, Kouji Segawa, Seiki Komiya, Yoichi Ando, J. M. Tranquada, and D. N. Basov, "Possibility of magnetic-field-induced reconstruction of the Fermi surface in underdoped cuprates: Constraints from infrared magneto-optics", Phys. Rev. B **81**, 064510 (2010).

45. A. D. LaForge, W. J. Padilla, K. S. Burch, Z. Q. Li, A. A. Schafgans, Kouji Segawa, Yoichi Ando, and D. N. Basov, "Magnetic field induced modification of superfluid density and interplane spectral weight in $YBa_2Cu_3O_y$", Phys. Rev. B **79**, 104516 (2009).

46. A. A. Schafgans, K. W. Post, A. A. Taskin, Yoichi Ando, Xiao-Liang Qi, B. C. Chapler, and D. N. Basov, "Landau level spectroscopy of surface states in the topological insulator $Bi_{0.91}Sb_{0.09}$ via magneto-optics", Phys. Rev. B **85**, 195440 (2012).

47. A. D. LaForge, A. Frenzel, B. C. Pursley, Tao Lin, Xinfei Liu, Jing Shi, and D. N. Basov, "Optical characterization of Bi_2Se_3 in a magnetic field: Infrared evidence for magnetoelectric coupling in a topological insulator material", Phys. Rev. B **81**, 125120 (2010).

48. E. Helgren, L Zeng, K. Burch, D. Basov, and F. Hellman, "Field- and concentration-tuned scaling of a quantum phase transition in a magnetically doped semiconductor", Phys. Rev. B **73**, 155201 (2006).

49. http://www.physics.umd.edu/DrewGroup/Research.html, (2014)

50. J. Cerne, D. C. Schmadel, L. B. Rigal, and H. D. Drew, "Measurement of the infrared magneto-optic properties of thin-film metals and high temperature superconductors" Rev. Sci. Instrum. **74**, 4755 (2003).

51. G. S. Jenkins, D. C. Schmadel, and H. D. Drew, "Simultaneous measurement of circular dichroism and Faraday rotation at terahertz frequencies utilizing electric field sensitive detection via polarization modulation", Rev. Sci. Instrum. **81**, 083903 (2010).

52. A. B. Sushkov, R. V. Aguilar, S. Park, S.-W. Cheong, and H. D. Drew, "Electromagnons in Multiferroic YMn_2O_5 and $TbMn_2O_5$," Phys. Rev. Lett. **98**, 027202 (2007).

53. R. Valdés Aguilar, A. B. Sushkov, C. L. Zhang, Y. J. Choi, S.-W. Cheong, and H. D. Drew, "Colossal magnon-phonon coupling in multiferroic $Eu_{0.75}Y_{0.25}MnO_3$," Phys. Rev. B **76**, 060404 (2007).

54. G. S. Jenkins, D. C. Schmadel, A. B. Sushkov, H. D. Drew, M. Bichler, G. Koblmueller, M. Brahlek, N. Bansal, and S. Oh, *"Dirac cone shift of a passivated topological Bi_2Se_3 interface state,"* Phys. Rev. B **87**, 155126 (2013).

55. G. S. Jenkins, A. B. Sushkov, D. C. Schmadel, M.-H. Kim, M. Brahlek, N. Bansal, S. Oh, and H. D. Drew, *"Giant plateau in the terahertz Faraday angle in gated Bi_2Se_3"*, Phys. Rev. B **86**, 235133 (2012).

56. G. S. Jenkins, A. B. Sushkov, D. C. Schmadel, N. P. Butch, P. Syers, J. Paglione, and H. D. Drew, *"Terahertz Kerr and reflectivity measurements on the topological insulator Bi_2Se_3*", Phys. Rev. B **82**, 125120 (2010).

57. G. S. Jenkins, D. C. Schmadel, P. L. Bach, R. L. Greene, X. Béchamp-Laganière, G. Roberge, P. Fournier, H. Kontani, and H. D. Drew, *"Origin of the anomalous Hall effect in the overdoped n-type superconductor $Pr_{2-x}Ce_xCuO_4$: Current-vertex corrections due to antiferromagnetic fluctuations*", Phys. Rev. B **81**, 024508 (2010).

58. G. S. Jenkins, D. C. Schmadel, A. B. Sushkov, G. D. Gu, H. Kontani, and H. D. Drew, *"Terahertz Hall measurements on optimally doped single-crystal $Bi_2S_2CaCu_2O_{8+x}$*", Phys. Rev. B **82**, 094518 (2010).

59. http://www.ifp.tuwien.ac.at/spectroscopy/research/, (2014)

60. A. M. Shuvaev, G. V. Astakhov, G. Tkachov, C. Brüne, H. Buhmann, L. W. Molenkamp, and A. Pimenov "Terahertz quantum Hall effect of Dirac fermions in a topological insulator " Phys. Rev. B **87**, 121104(R) (2013).

61. A. M. Shuvaev, G. V. Astakhov, C. Brüne, H. Buhmann, L.W. Molenkamp and A. Pimenov, "Terahertz magneto-optical spectroscopy in HgTe thin films", Semicond. Sci. Technol. **27**, 124004 (2012).

62. A. M. Shuvaev, G. V. Astakhov, A. Pimenov, C. Brüne, H. Buhmann, and L. W. Molenkamp "Giant Magneto-Optical Faraday Effect in HgTe Thin Films in the Terahertz Spectral Range" Phys. Rev. Lett. **106**, 107404 (2011).

63. A. M. Vasiliev, L. A. Prozorova, L. E. Svistov, V. Tsurkan, V. Dziom, A. Shuvaev, Anna Pimenov, and A. Pimenov "ESR of the quasi-two-dimensional antiferromagnet $CuCrO_2$ with a triangular lattice", Phys. Rev. B **88**, 144403 (2013).

64. A. M. Kuzmenko, A. Shuvaev, V. Dziom, Anna Pimenov, M. Schiebl, A. A. Mukhin, V. Yu. Ivanov, L. N. Bezmaternykh, and A. Pimenov, "Giant gigahertz optical activity in multiferroic ferroborate", Phys. Rev. B **89**, 174407 (2014)

65. A. M. Shuvaev, A. A. Mukhin, and A. Pimenov, "Magnetic and magnetoelectric excitations in multiferroic manganites", J. Phys.: Condens. Matter **23**, 113201 (2011).

66. A. Pimenov, S. Engelbrecht, A. M. Shuvaev, B. B. Jin, P. H. Wu, B. Xu., L. X. Cao, and E. Schachinger, "Terahertz conductivity in $FeSe_{0.5}Te_{0.5}$ superconducting films", New J. Phys. **15**, 013032 (2013).

67. M. Dressel, N. Drichko, B. Gorshunov, and A. Pimenov, "THz Spectroscopy of Superconductors", IEEE Selected Topics in Quantum Electronics **14**, 399 (2008).

68. A. Schneider, A. Shuvaev, S. Engelbrecht, S. O. Demokritov, and A. Pimenov "Electrically Excited Inverse Electron-Spin-Resonance in a Split-Ring Metamaterial Resonator" Phys. Rev. Lett. **103**, 103907 (2009).

69. A. Pimenov, A. Loidl, K. Gehrke, V. Moshnyaga, and K. Samwer "Negative Refraction Observed in a Metallic Ferromagnet in the Gigahertz Frequency Range", Phys. Rev. Lett. **98**, 197401 (2007).

70. M. Neshat · N. P. Armitage, Developments in THz Range Ellipsometry, J. Infrared Milli Terahz Waves **34**, 682–708 (2013).

71. LiDong Pan, Se Kwon Kim, A. Ghosh, Christopher M. Morris, Kate A. Ross, Edwin Kermarrec, Bruce D. Gaulin, S. M. Koopayeh, Oleg Tchernyshyov, N. P. Armitage, Low-energy electrodynamics of novel spin excitations in the quantum spin ice Yb2Ti2O7, Nat. Commun. 5: 4970 (2014).

72. N. P. Armitage, Constraints on Jones transmission matrices from time-reversal invariance and discrete spatial symmetries, Phys. Rev. B 90, 035135 (2014).

73. C. M. Morris, R. Valdés Aguilar, A. Ghosh, S. M. Koohpayeh, J. Krizan, R. J. Cava, O. Tchernyshyov, T. M. McQueen, N. P. Armitage, Hierarchy of bound states in the one-dimensional ferromagnetic Ising chain $CoNb_2O_6$ investigated by high-resolution time-domain terahertz spectroscopy, Phys. Rev. Lett. **112**, 137403 (2014).

74. LJ Sandilands, AA Reijnders, M Kriener, K Segawa, S Sasaki, Y Ando, et al., Doping- dependent charge dynamics in CuxBi2Se3, Physical Review B **90** (9), 094503 (2014).

75. H. Schmid, "*Multi-ferroic magnetoelectrics*" Ferroelectrics, **162**, 317 (1994)

76. N.A. Hill, "*Why are there so few magnetic ferroelectrics*?", J. Phys. Chem. B **104**, 6694 (2000).

77. C.W. Nan, M.I. Bichurin, S. Dong, D. Viehland, G. Srinivasan, "*Multiferroic magnetoelectriccomposites: Historical perspective, status, and future directions*", J. Appl. Phys. **103**, 031101 (2008).

78. C.A.F. Vaz, J. Hoffman, C.H. Ahn, R. Ramesh, "*Magnetoelectric coupling effects in multiferroic complex oxide composite structures*", Adv. Mater. **22**, 2900 (2010)

79. B.G. Ueland, J.W. Lynn, M. Laver, Y.J. Choi, S.W. Cheong, "*Origin of electric field induced magnetization in multiferroic HoMnO3*", *Phys. Rev. Lett.* **104**, 147204 (2010)

80. N. Kida, Y. Tokura, *Terahertz magnetoelectric response via electromagnons in magnetic oxides*, arXiv:1107.0428v1 [cond-mat.str-el] (submitted to Journal of Magnetism and Magnetic Materials in July 5, 2011).

81. T. H. O'Dell, *The Electrodynamics of Magneto-Electric Media*. (North Holland, Amsterdam, 1970).

82. J.-P. Rivera, *A short review of the magnetoelectric effect and related experimental techniques on single phase (multi-) ferroics*, Eur. Phys. J. B **71** (3), 299-313 (2009).

83. T. Kimura, T. Goto, H. Shintani, K. Ishizaka, T. Arima, Y. Tokura, *Magnetic control of ferroelectric polarization* , Nature **426** (2003) 55.

84. N. Hur, S. Park, P.A. Sharma, J.S. Ahn, S. Guha, and S-W. Cheong, "*Electric polarization reversal and memory in a multiferroic material induced by magnetic fields*", Nature 429, 392 (2004).

85. N. A. Spaldin and M. Fiebig, "*The renaissance of Magnetoelectric Multiferroics*" , Science, **309**, 391 (2005).

86. N. Hur, S. Park, P. A. Sharma, S. Guha, S-W. Cheong, *"Colossal magnetodielectric effects in* $DyMn_2O_5$", Phys. Rev. Lett. **93**, 207 (2004).

87. T. Goto, T. Kimura, G. Lawes, A. P. Ramirez, and Y. Tokura, "*Ferroelectricity and Giant Magnetocapacitance in Perovskite Rare-Earth Manganites",* Phys. Rev. Lett. **92**,257201(2004).

88. Y. Tokunaga, N. Furukawa1, Hideaki Sakai, Y. Taguchi, T. Arima, and Y. Tokura1, "*Composite domain walls in a multiferroic perovskite ferrite*", Nature Materials **8**, 558 (2009).

89. Y. Tokura, S. Seki, *Multiferroics with Spiral Spin Orders* , Adv. Mater. 22 (2010) 1554.

90. T. Arima, *Spin-Driven Ferroelectricity and Magneto-Electric Effects in Frustrated Magnetic Systems*, J. Phys. Soc. Jpn. 80 (2011) 052001.

91. S-W. Cheong and M. Mostovoy, "*Multiferroics: a magnetic twist for ferroelectricity*", Nature Materials **6**, 14 (2007).

92. W. S. Weiglhofer and A. Lakhtakia, *Introduction to Complex Mediums for Optics and Electromagnetics*. (SPIE Optical Engineering Press, Bellingham, Wash., 2003).

93. Y. Takahashi, R. Shimano, Y. Kaneko, H. Murakawa, and Y. Tokura, *Magnetoelectric resonance with electromagnons in a perovskite helimagnet*, Nature Physics **8**, 121–125 (2012).

94. S. Miyahara, and N. Furukawa, *Nonreciprocal Directional Dichroism and Toroidalmagnons in Helical Magnets*, J. Phys. Soc. Jpn. **81**, 023712 (2012).

95. T. Arima, *Magneto-electric optics in non-centrosymmetric ferromagnets* , J. Phys.: Condens.Matter **20** (2008) 434211.

96. V. G. Veselago, *Electrodynamics of substances with simultaneously negative values of* eps and μ, Soviet Physics USPEKHI **10**, 509 (1968).

97. J. B. Pendry, *Negative refraction*, Contemporary Physics 45, **191** (2004).

98. W.Eerenstein, N.D. Mathur, J.F. Scott, Nature **442**/7104, 759 (2006).

99. G. A Smolensky, R. V. Pisarev, and I. G. Siniy, "Light Birefringence in magnetically ordered crystals", Usp. Fiz. Nauk, 116(2) 231-269 (1975).

100. Yoon Seok Oh, Sergey Artyukhin, Jun Jie Yang, Vivien Zapf, Jae Wook Kim, David Vanderbilt, and Sang-Wook Cheong, "Non-hysteretic colossal magnetoelectricity in a collinear antiferromagnet", Nature Communications 5, 3201 (2014).

101. A. Shuvaev, F. Mayer, A. Loidl, A. A. Mukhin and A. Pimenov, *High-Frequency Electromagnon in GdMnO*, ArXiv 1008.2064v1 (2010).

102. D. E. Aspnes, ''*The accurate determination of optical properties by ellipsometry*,'' in *Handbook of Optical Constants of Solids*, E. D. Palik, ed. (Academic Press, Inc., New York, 1985), pp. 89–112.

103. M. Schubert, *Theory and Application of Generalized Ellipsometry*, Chapter 9 in Handbook of Ellipsometry, edited by G. Irene and H. Tompkins (Noyes, Park Ridge, NJ, 2004).

104. G. E. Jellison, Jr., ''*Spectroscopic ellipsometry data analysis: measured versus calculated quantities*,'' Thin Solid Films **313-314**, 33–39 (1998).

105. U. Rossow and W. Richter, "*Spectroscopic Ellipsometry",* in *Optical Characterization of Epitaxial Semiconductor Layers*, Eds. G. Bauer and W. Richter, (Springer 1996), pp. 68-128.

106. H. Fujiwara, *Spectroscopic Ellipsometry: Principles and Applications* (John Wiley & Sons, 2007).

107. T. Hofmann, U. Schade, C. M. Herzinger, P. Esquinazi, and M. Schubert, *Terahertz generalized Mueller-matrix ellipsometry* , SPIE Vol. **6120**, 61200D (2006).

108. T. Hofmann, C. M. Herzinger, A. Boosalis, T. E. Tiwald, J. A. Woollam, and M. Schubert, "*Variable-wavelength frequency-domain terahertz ellipsometry*," Rev. Sci. Instrum. **81**, 023101 (2010).

109. A. Röseler, *Infrared Spectroscopic Ellipsometry* (Akademie, Berlin, 1992).

110. M. Schubert, B. Rheinla¨nder, B. Johs, C. M. Herzinger, and J. A. Woollam, ‘‘*Extension of rotating analyzer ellipsometry to generalized ellipsometry: determination of the dielectric function tensor from uniaxial TiO2*,’’ J. Opt. Soc. Am. A **13**, 875–883 (1996).

111. M. Schubert, T. E. Tiwald, and J. A. Woollam, ‘‘*Explicit solutions for the optical properties of arbitrary magneto-optic materials in generalized ellipsometry*,’’ Appl. Opt. **38**, 177– 187 (1999).

112. M. Schubert, ‘‘*Polarization-dependent optical parameters of arbitrarily anisotropic homogeneous layered systems*,’’ Phys. Rev. B **53**, 4265–4274 (1996).

113. T. E. Tiwald and M. Schubert, ‘‘*Measurement of rutile TiO2 from 0.148 to 33 mm using generalized ellipsometry*,’’ in *Optical Diagnostic Methods For Inorganic Materials II*, L. M. Hanssen, ed., Proc. SPIE **4103**, 19–29 (2000).

114. M. Schubert, *Another century of ellipsometry,* Annalen der Physik **15**, 480-497 (2006).

115. M. Schubert, A. Kasic, T. Hofmann, V. Gottschalch, J. Off, F. Scholz, E. Schubert, H. Neumann, I. Hodgkinson, M. Arnold, W. Dollase, and C. M. Herzinger, *Generalized ellipsometry of complex mediums in layered systems*, SPIE Vol. **4806**, 264 (2002).

116. H. Fujiwara, *Spectroscopic Ellipsometry : Principles and Applications*. (John Wiley & Sons, Chichester, England ; Hoboken, NJ, 2007).

117. M. Schubert, T. Hofmann, and C. M. Herzinger, "*Generalized far-infrared magneto -optic ellipsometry for semiconductor layer structures: determination of free -carrier effective-mass,mobility, and concentration parameters in n-type GaAs***",** J. Opt. Soc. Am. A, **20**, No. 2 (February 2003).

118. D. W. Berreman, *Optics in Stratified and Anisotropic Media: 4 × 4-Matrix Formulation* , J. Opt. Soc. Am. **62**, 502-510 (1972).

119. R. M. A. Azzam and N. M. Bashara, *Ellipsometry and Polarized Light*. (North -Holland, Amsterdam, 1977).

120. This design has been described in the Theses of Ken Burch' Grad Student: "Optical spectroscopy of Novel Materials", by Anjan A. Reijnders (2014).